frontiers | Frontiers in Earth Science

TYPE Original Research
PUBLISHED 24 April 2025
DOI 10.3389/feart.2025.1573609

OPEN ACCESS

EDITED BY
Mao-Wen Yuan,
China University of Geosciences, China

REVIEWED BY
Yuanji Li,
Heilongjiang University of Science and Technology, China
Yunpeng Yu,
China Aero Geophysical Survey and Remote Sensing Center for Natural Resources, China

*CORRESPONDENCE
Xiaoneng Luo,
lxnbriug@126.com

RECEIVED 09 February 2025
ACCEPTED 10 March 2025
PUBLISHED 24 April 2025

CITATION
Luo X, Peng S, Li Z, He F, Li X and Zhang Z (2025) Petrography and geochemistry of sandstones from the middle Jurassic Zhiluo Formation in the northern margin, Ordos Basin: implications for provenance, tectonic setting, paleoweathering, paleoclimate, and sandstone-type uranium mineralization. *Front. Earth Sci.* 13:1573609. doi: 10.3389/feart.2025.1573609

Petrography and geochemistry of sandstones from the middle Jurassic Zhiluo Formation in the northern margin, Ordos Basin: implications for provenance, tectonic setting, paleoweathering, paleoclimate, and sandstone-type uranium mineralization

Xiaoneng Luo[1,2]*, Suping Peng[1], Ziying Li[2], Feng He[2], Xide Li[2] and Zilong Zhang[2]

[1]State Key Laboratory of Coal Resources and Safe Mining, China University of Mining and Technology, Beijing, China, [2]Beijing Research Institute of Uranium Geology, China National Nuclear Corporation (CNNC), Beijing, China

This study aims to analyze the provenance of Middle Jurassic Zhiluo Formation sandstones exposed by drilling in the northern Ordos Basin (Bayingqinggeli area) and reconstruct the tectonic setting, paleoclimate, and paleoweathering conditions of their source rocks through integrated petrographic and geochemical analyses (major, trace, and rare earth elements). Comprehensive evaluation of mineral assemblages and geochemical signatures reveals that the detrital components of the studied sandstones were predominantly derived from multiple recycled felsic (granitic) igneous sources, with subordinate contributions from intermediate igneous (granodioritic), metamorphic (gneissic), and mafic igneous (andesitic) provenances. Diagnostic elemental ratios including La/Sc, Th/Sc, and Co/Th demonstrate a principal derivation from felsic lithologies (granites and gneisses) coupled with recycled quartzose sedimentary sources. Chondritenormalized REE patterns exhibit light REE (LREE) enrichment, flat heavy REE (HREE) distributions, and pronounced negative Eu/Eu*anomalies, showing close affinity to Upper Continental Crust (UCC) characteristics dominated by felsic lithologies. Geochemical proxies and trace element ratios (e.g., Th/U, Th/Sc) indicate that the source area underwent moderate to intense chemical weathering, primarily under arid climatic conditions with intermittent episodes of warm, semi-humid to humid paleoenvironments. The integrated dataset further suggests a complex

exhumation history involving cratonic basement uplift and reactivation of Paleozoic orogenic belts during the Mesozoic era.

KEYWORDS

element geochemistry, provenance analysis, middle Jurassic sandstone, paleoenvironment, Ordos Basin

1 Introduction

The mineralogical and chemical composition of clastic sedimentary rocks is significantly shaped by a multitude of factors, such as weathering processes, modes of transportation, paleoclimatic conditions, tectonic environments, and the diagenetic alterations of the parent rocks (McLennan and Taylor, 1980; Pettijohn et al., 1987; McLennan et al., 1993; Cox et al., 1995). Modal analysis of detrital framework grains in clastic sedimentary rocks has been employed to ascertain their provenance (Basu et al., 1975; Dickinson and Suczek, 1979; Dickinson et al., 1983; Critelli et al., 2003). and tectonic provenance (Dickinson, 1970; Basu et al., 1975; Dickinson et al., 1983). Furthermore, the concentrations of major, trace, and rare earth elements in clastic sedimentary rocks can be utilized as proxies to infer the provenance (Taylor and McLennan, 1985; Roser and Korsch, 1988; Cullers, 2000; Augustsson et al., 2023), and to reconstruct the tectonic setting (Dickinson and Suczek, 1979; Bhatia, 1983; Bhatia and Crook, 1986; Kroonenberg, 1994; Verma and Armstrong-Altrin, 2013; Verma and Armstrong-Altrin, 2016), paleoclimate (Nesbitt and Young, 1982), and paleo-weathering (McLennan et al., 1993; Cox et al., 1995; Fedo et al., 1995; Nesbitt and Young, 1982; Ivanova et al., 2015) in the source area (rocks). Such studies have been widely proved and applied by many authors (e.g., Wanas and Abdel-Maguid, 2006; Zaid, 2012; Armstrong-Altrin et al., 2015; Armstrong-Altrin et al., 2017; Löwen et al., 2018; Alqahtani and Khalil, 2019; Alqahtani and Khalil, 2021; Sallam and Wanas, 2019; Moghaddam et al., 2020; Ma et al., 2021; Wanas and Assal, 2021; Augustsson et al., 2023; Quasim et al., 2023).

Sandstone-type uranium deposits in sedimentary basins are a prominent category of uranium resources with important implications for national energy security. The sedimentary paleogeographic context of basin development is a major controlling factor in the enrichment of sandstone-type uranium deposits. The accumulation of structural changes over time frequently serves as a pathway for the movement of uranium-containing oxidising fluids. As a result, paleoenvironmental reconstruction and provenance analysis are critical components in the discovery, delineation, exploration, and assessment of the potential for uranium reservoirs in uranium-rich basins. This research area is not only a topical and Frontier subject in sedimentary basin studies, but it also addresses a critical geological issue that limits the successful exploitation of sandstone-type uranium deposits.

In recent years, numerous academics have worked extensively on the provenance of the Jurassic Zhiluo Formation in the northern Ordos Basin. Previous research has used petrological, geochemical, U-Pb zircon dating, and heavy mineral analysis approaches to answer the provenance problem of the Zhiluo Formation in the basin's northern region. However, the controversy over the Jurassic in the northern Ordos Basin mainly lies in the unclear relationship between provenance and uranium source. Is uranium source from a uranium rich rock mass in the erosion source area? Alternatively, is it the activation and migration of uranium in the rock of the target layer itself? Or is this due to the influx of deep high-uranium fluids? Therefore, it is necessary to conduct in-depth research on Jurassic provenance in this area and explore the development of the prototype basin. Provenance is the link between the sedimentary basins and orogenic belts. Conducting provenance analysis on sedimentary basins helps to understand their sedimentary filling and structural evolution and is an important means of reconstructing paleogeographic environments and restoring the interaction between basin mountain systems. At present, there are relatively few systematic source analyses of the Jurassic system in the northern Ordos Basin, and the source analysis methods are relatively single, lacking a comprehensive regional systematic source study that combines multiple methods. The geochemical characteristics of sediments are controlled by the composition of the source rocks and influenced by chemical weathering processes. The climatic conditions of the source area determine the intensity of chemical weathering. Therefore, the geochemical characteristics of sedimentary rocks can serve as indicators of source rock features, geochemical weathering processes, and palaeoclimatic reconstruction. Despite the aforementioned results, there has been no previous discussion of the sources of clastic rocks in the Zhiluo Formation, palaeo-tectonic setting, palaeoclimate, palaeo-weathering, or paleogeography of their source rocks. This research seeks to elucidate the origin of the sandstones from the Zhiluo Formation while also redefining the tectonic context, paleoclimate, and paleo-weathering conditions of their source rocks. To fulfil these objectives, a comprehensive mineralogical–geochemical study was conducted on the sandstones of the Zhiluo Formation.

2 Geological setting

Ordos Basin is the second largest basin in China, neighbouring Wolf Mountain and Daqing Mountain in the north; Luliang Mountain in the east; Weibei in the south; and Helan Mountain in the west. The basin belongs to the North China Craton, located in the western part of the North China Craton, which is a multi-overlapping basin within the unstable Craton, formed by the intersection, superposition and composite of the three major tectonic domains of the Paleo-Asia, Tethys and the Pacific Rim under the action of the Paleo-Asian, Tethys and Pacific Rim tectonic domains since it has been accepted for deposition in the Middle and Late Proterozoic era on the basis of the North China Craton. The basin is surrounded by orogenic belts, from north to south for the Tianshan-Xingmeng fold belt, the Alashan Massif, the corridor transition zone and the Qilian-Qinling fold belt. Since the

development stage of the sedimentary cover, the formation and evolution of the basin is obviously influenced and controlled by the three major tectonic domains of the Paleo-Asian Ocean, the Tethys Ocean and the coastal Pacific Ocean. The basin is surrounded by strong activity, with intensive folding and fracture traces, and relatively stable magmatic activities, with the main forms of uplift, depression, and broad and slow folding.

Since the Mesozoic, the Ordos Basin can be divided into six tertiary tectonic units, namely, the Yimeng uplift, the Yishan slope, the Tianhuan syncline, the western margin retrograde zone, the west Jin flexure zone, and the north Weibei uplift, among which the three tectonic units of the Yimeng uplift, the Yishan slope, and the Tianhuan syncline are close to the environment of the working area of uranium mineralisation. The Yishan slope is the main tectonic unit of the Ordos Basin, occupying most of the basin. The uranium mineralisation zone in the northern part of the Ordos Basin is located in the Dongsheng-Jingbian monocline of the Yimeng uplift and the Yishan slope, both of which have a direct influence on the Mesozoic sedimentation and uranium mineralisation.

The cover layers developed in the basin include Mesozoic Triassic (T), Jurassic (J), Lower Cretaceous ($_{K1}$), and Cenozoic Paleoproterozoic (E), Neoproterozoic (N), and Quaternary (Q), and there is a big difference of development of the various strata horizontally and vertically, among which the Triassic, the Jurassic, and the Lower Cretaceous are the main depositional strata in the basin. The Jurassic is exposed in a north-south belt in the eastern part of the basin, and dips under the Lower Cretaceous to the west and south-west, which is an important coal-bearing stratum in the basin, and is also the main target stratum for searching for uranium ore. The Lower Cretaceous is widely distributed in the northern part of the basin, and it is the main target layer for finding uranium ore in the western part of the basin. The Palaeoproterozoic and Neoproterozoic systems are sporadically exposed, while the Quaternary system is widely distributed in the central and southern parts of the basin.

3 Sampling and methodology

3.1 Sample collection and processing

This study was conducted using a combination of field observations and laboratory methodologies. In this study, samples were collected from two boreholes of the Bayingqinggeli uranium deposit, with a total of 27 samples collected, including green and gray medium coarse sandstones, for whole-rock geochemical analysis. Detailed sampling locations are shown in Figure 1. To ensure that the samples could represent the geochemical characteristics of the formation itself, suitable fresh samples were collected based on core observations, avoiding possible influencing factors such as weathering, alteration, and recycling. Indoor, take an appropriate amount of the collected sample and grind it to 200 mesh, send it to the laboratory for analysis, and complete the processing in a pollution-free environment. Composition analyses of the main, trace, and rare earth elements were conducted at the Analysis and Testing Research Center of the Beijing Research Institute of Uranium Geology.

3.2 Methods of analysis

Major element concentrations were obtained using an X-ray fluorescence spectrometer (AB-104 L, PW2404) as subsequent analytical procedures: First, each powdered sample weighed 0.4 g and was equably stirred in Ni-pots with anhydrous $Li_2B_4O_7$ and dissolved with NH_4Br liquid of 120 mg/mL and a suitable oxidant; second, the Ni-pots were placed on the CLAISSIE sampling machine for liquation according to the procedure presented. Afterwards, the high-temperature melts were placed in moulds and finally encased in plastic bags for preservation in desiccators. The X-ray data were converted into concentrations using a computer program based on the matrix correction method. The accuracy was estimated to be <2% for all the major element oxides.

Trace element concentrations, including REEs, were measured by an ELEMENT XR ICP-MS using the following procedure. First, powders were weighed (25 mg) and placed in high pressure-resistant beaker, with a 1:1 mixture of HF-HNO_3 and heated for 24 h at 80°C to be evaporated. Second, 1.5 mL HNO_3, 1.5 mL HF, and 0.5 mL $HClO_4$ were added, respectively, after solutions were evaporated to nearly dry, and the beakers with solutions were capped for digestion within a high-temperature oven at 180°C for at least 48 h until the samples were completely dissolved. Finally, the solutions were diluted with 1% HNO_3 to 50 mL for determination. The accuracy was estimated to be 5% for all trace elements.

3.3 Geochemical indices

Eu/Eu* was calculated as equal to $(Eu)_{cn}/[(Sm)_{cn} \times (Gd)_{cn}] \times 0.5$ (McLennan, 1989), and Ce/Ce* was calculated as equal to $(Ce_{cn})/[(La_{cn} + Pr_{cn})] \times 0.5$. Here, cn refers to the chondrite-normalised values of the element (Taylor and McLennan, 1985). Chemical weathering indices encompass several key metrics, including the Chemical Index of Alteration (CIA), the Chemical Index of Weathering (CIW), the Plagioclase Index of Alteration (PIA), and the Index of Compositional Variability (ICV). These indices are essential for assessing the degree of chemical weathering and the alteration of mineral compositions in geological studies (Table 1). In this research, all weathering indices, including CIA, PIA, ICV, and CIW, were utilized due to their significance in evaluating palaeo-weathering within the source area and elucidating the compositional variations of the examined sandstones. Specifically, CIA, PIA, and CIW values of 60, 60–80, and greater than 80 indicate low to moderate and strong weathering intensities, respectively (Nesbitt and Young, 1982; Fedo et al., 1995). The ICV values provide valuable insights into the compositional variations of source rocks resulting from chemical weathering. Specifically, an ICV value greater than 1 indicates the presence of minerals such as feldspars, amphiboles, and pyroxenes, which are indicative of chemical weathering processes. Conversely, an ICV value less than 1 suggests the dominance of alteration products, including kaolinite, illite, and muscovite, within the source rocks (Cox et al., 1995; Cullers, 2000). The UCC-normalised diagram of trace elements was constructed according to Rudnick and Gao (2003). The chondrite normalisation values of RRE were obtained from Taylor and McLennan (1985), and the average PAAS normalisation values were obtained from McLennan (1989). The discriminant

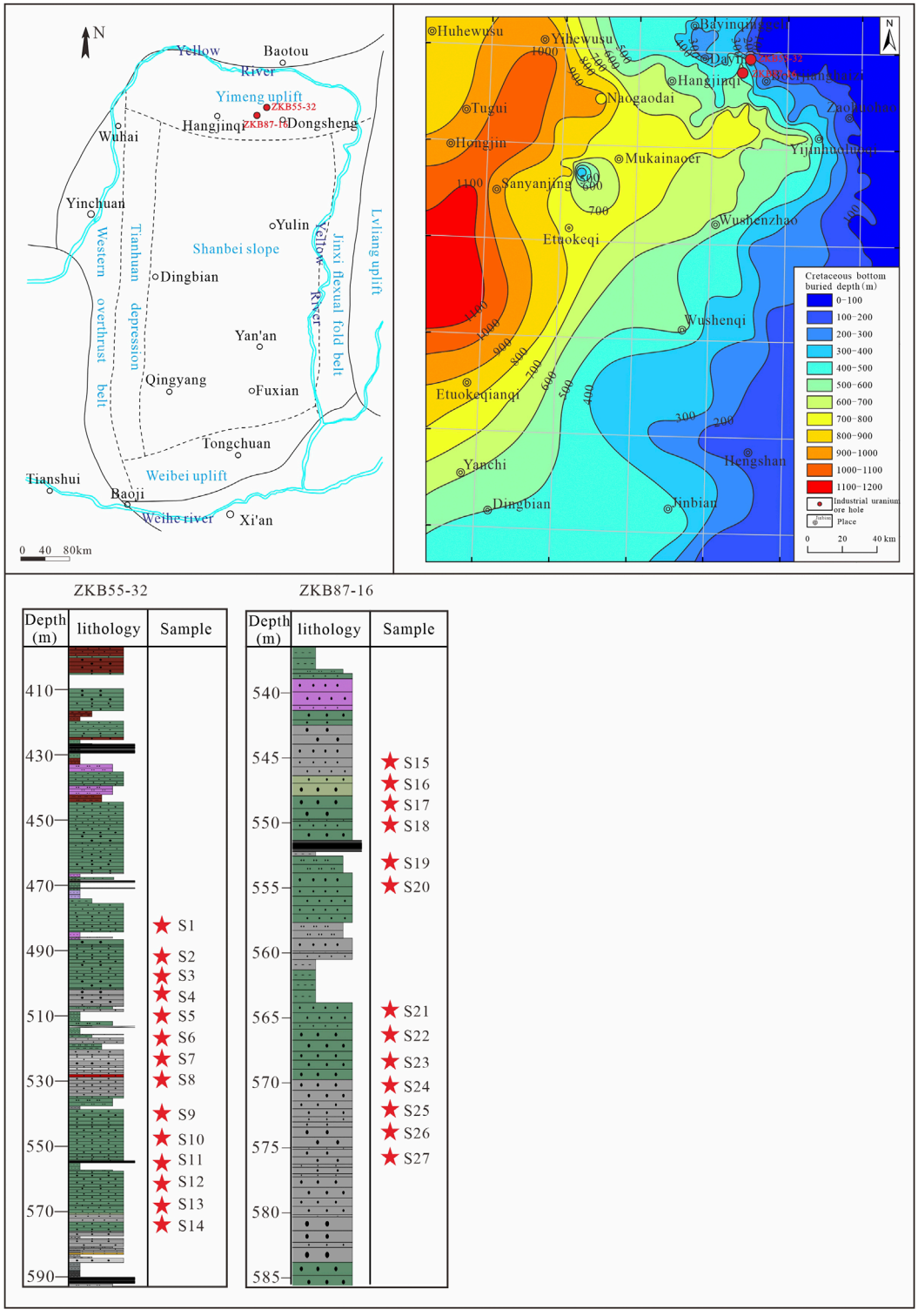

FIGURE 1
Geological map and sampling location map of the northern Ordos Basin.

functions of Roser and Korsch (1988) were applied to discriminate the provenance of sandstones, whereas the discriminant functions (based on major elements) of Bhatia (1983), Roser and Korsch (1986), and Bhatia and Crook (1986) were used to infer the tectonic setting. In addition, the new discriminant functions of Verma and Armstrong-Altrin (2013), Analyses of major oxides in high- and low-silica sandstones and shales have been utilized to differentiate among three primary tectonic environments:

TABLE 1 Summary of published weathering indices considered in this study.

Proxies	Formula	Sources
CIA	$Al_2O_3/(Al_2O_3 + CaO^* + Na_2O + K_2O) \times 100$	Nesbitt and Young (1982)
PIA	$(Al_2O_3 - K_2O)/(Al_2O_3 + CaO^* + Na_2O - K_2O) \times 100$	Fedo et al. (1995)
CIW	$Al_2O_3/(Al_2O_3 + Ca_2O^* + Na_2O) \times 100$	Harnois (1988)
CIX	$Al_2O_3/(Al_2O_3 + Na_2O + K_2O) \times 100$	
ICV	$(Fe_2O_3 + K_2O + Na_2O + CaO + MgO + TiO_2)/Al_2O_3$	Cox et al. (1995)

$CaO_{corrected}$ = mol CaO − 10/3 mol P_2O_5, the CaO in the apatite was subtracted. If mol $CaO_{corrected} \leq Na_2O$, $CaO^* = CaO_{corrected}$; if $CaO_{corrected} > Na_2O$, $CaO^* = Na_2O$.

island or continental arc, continental rift, and collision zones. The newly developed discriminant functions hold significant importance for their application to the analyzed sandstones and shales, particularly due to their effectiveness in addressing chemical alterations associated with weathering, recycling, and diagenesis (Verma and Armstrong-Altrin, 2013). Samples with elevated levels of carbonate and/or iron cement were omitted from the analysis, as the presence of CaO and/or iron cement may lead to erroneous interpretations concerning provenance and tectonic context (Cullers, 2000).

4 Results

4.1 Petrological characteristics

Observation of field outcrops and drill core samples shows that the sandstone of the Zhiluo Formation in the Bayinqinggeli area of the northern Ordos Basin is generally gray green to green in color, with strong vertical heterogeneity (Figure 2), indicating frequent changes in sedimentary environment. Microscopic thin section identification shows that the core samples of boreholes 55-32 and 87-16 are mainly composed of quartz, feldspar, carbonate minerals (mainly calcite), and clay minerals, with a small amount of pyrite (Figure 2).

4.2 Geochemistry

The results of major (oxides), trace, and rare earth elements, and loss of ignition (LOI) of the studied sandstone samples are listed in Tables 2–4.

4.2.1 Major oxides geochemistry

The main elemental analyses of the Bayinqinggeli samples in the Ordos Basin are presented in Table 2. The major element concentrations of the 55-32 core and the 87-16 core are expressed as weight percentages of oxides The major element oxides SiO_2 and Al_2O_3 constitute the dominant oxides, with contents ranging from 60 to 72.31 wt% and 11.49–14.99 wt% in the 55–32 core and from 68.91 to 74.46 wt% and 11.11–13.12 wt% in the 87–16 core. The concentrations of Fe_2O_3, MgO and CaO in the 55–32 core vary between 2.16 and 6.89 wt%, 1.09–2.36 wt% and 0.708–1.66 wt%, respectively. In the 87-16 core, they range from 1.69 to 5.66 wt%, 1.08–1.98 wt% and 0.614–1.84 wt%, respectively. The concentrations of Na_2O and K_2O in the 55–32 core vary between 0.996–2.46wt% and 2.83–3.71 wt%, respectively. In the 87–16 core, they range from 1.1 to 1.98 wt% and 2.66–3.49 wt%, respectively. P_2O_5, TiO_2, and MnO were available in low concentrations of less than 2%.

The CIA values of the sandstone samples from boreholes to 55–32 and 87–16 (ranging from 65.49 to 76.08) were higher than those of PAAS (70) and UCC (52). Similarly, the PIA values of the studied sandstone (ranging from 73.71 to 88.49) were higher than those of PAAS (79) and UCC (53). Except for samples S6 and S8, whose CIW is below 80, the CIW of all the other samples is between 80 and 90, which is higher than those of PAAS (82) and UCC (58). According to the classification scheme of Sprague et al. (2009), the chemical classification of the samples from wells to 55–32 and 87–16 can be divided into claystone and siltstone (Figure 3a), which is consistent with the petrological classification (see Section 3.1). Correspondingly, the classification system of Herron (1988) shows that all samples can be classified as feldspathic sandstones and feldspathic heterosandstones, and most of the samples plot as feldspathic sandstones (Figure 3b).

4.2.2 Trace elements geochemistry

Concentrations of trace elements and their ratios (La/Th, La/Y, Y/Ni, Cr/V, Cr/Th, Th/Sc, Th/U, Sc/Cr, Zr/Sc, Th*10, Zr/10) for samples from Bayinqinggeli in the Ordos Basin are shown in Table 3. The trace elements were standardised by UCC (Figure 4). As shown in Table 3, Ba (content between 909 and 1,123 μg/g, average 1,004.21 ug/g) and U (content between 1.91 and 32.2 ug/g, average 12.26 ug/g) in sandstone drilled from 55-32 well and Ba (content between 840 and 1,099 μg/g, average 984.46 ug/g) and U (0.923~21.2 ug/g, average 7.12 ug/g) in sandstone drilled from 87-16 well, are enriched relative to UCC and higher than PAAS. Hf (1.04~4.95 ug/g, average 1.67 ug/g), Sc (5.46~13.6 ug/g, average 8.41 ug/g), Cr (30.1~117 ug/g, average 50.74 ug/g), Cu (4.73~21.6 ug/g, average 10.79 ug/g), Ni (8.5~26.1 ug/g, average 15.04 ug/g), Zn (34~78.9 ug/g, average 52.65 ug/g), Th (3.65~12.5 ug/g, average 5.94 ug/g), Zr (33.2~131 ug/g, average 53.36 ug/g) in the sandstone from 55-32 well, lower than the content of PAAS and UCC. Hf (0.974~3.09 ug/g, average 1.481 ug/g), Sc (5.14~9.36 ug/g, average 7.49 ug/g), Cr (26~56.7 ug/g, average 40.52 ug/g), Cu (2.71~12.2 ug/g, average 6.92 ug/g),

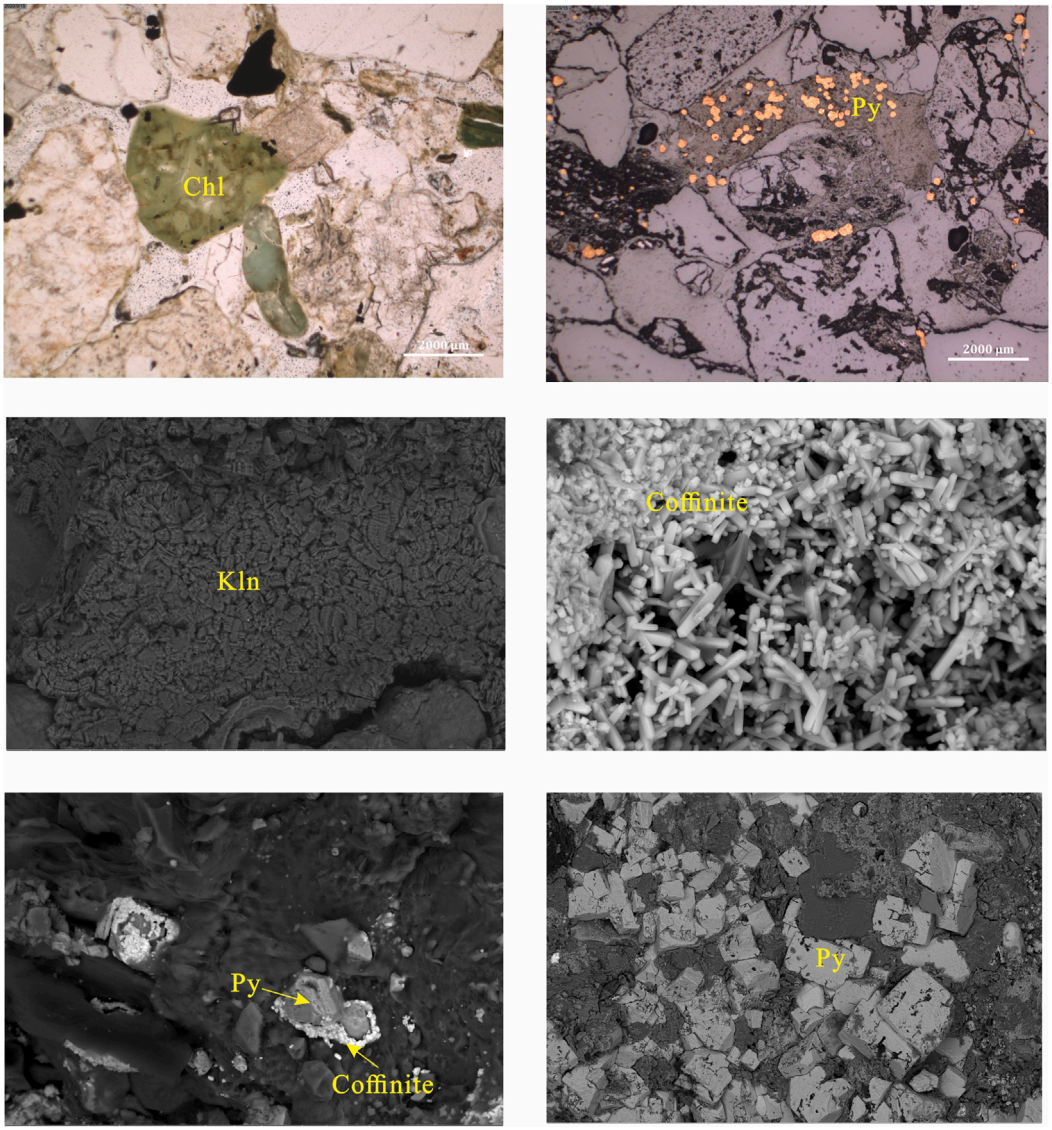

FIGURE 2
Microscopic photo of Zhiluo Formation sandstone in Bayinqinggeli area, northern Ordos Basin.

Ni (9.02~14.5 ug/g, average 11.53 ug/g), Zn (23.5~63.9 ug/g, average 37.06 ug/g), Th (3.26~9.02 ug/g, average 5.54 ug/g), Zr (30.4~106 ug/g, average 47.85 ug/g) in the sandstone from 87-16 well, lower than the content of PAAS and UCC. The Rb content (between 66.6 and 89.2 ug/g, with an average of 79.73 ug/g) and V content (between 42 and 209 ug/g, with an average of 88.83 ug/g) in the sandstone from 55-32 well, are similar to UCC content but lower than PAAS content. The Rb (between 66.3 and 99.4 ug/g, with an average of 82.25 ug/g) and V (between 43.6 and 215 ug/g, with an average of 113.68 ug/g) contents in the sandstone from 87-16 well, are similar to UCC content but lower than PAAS content. The Sr content in the sandstone of borehole 55-32 (274–367 μg/g, with an average of 319.86 ug/g) is similar to that of UCC and higher than that of PAAS. The Sr content in the sandstone from 87-16 well (between 230 and 331 μg/g, with an average of 289.46 ug/g) was similar to that of UCC and higher than that of PAAS.

4.2.3 Rare earth elements geochemistry

The rare earth element contents of the Bayinqinggeli samples from the Ordos Basin are listed in Table 4. The standardised pattern map of homogeneous globular meteorites (Figure 4) suggests that these sandstones may share the same source, and the model exhibits a slight positive Eu anomaly. Total rare earth elements (∑REE) in the sandstones of borehole 55-32 range from 95.97 to 284.99 ug/g, with an average value of 140.08ug/g, which is significantly lower than that of UCC and PAAS. total rare earth elements (∑REE) in the sandstones of borehole 87-16 range from 101.44 to 184.58 ug/g with an average of 132.05 ug/g, also significantly lower than the UCC and PAAS. In addition, the rare earth ligand pattern maps also indicate that the light rare earth elements (LREE, 55-32 samples ranged from 81.71 to 246.38 ug/g with an average of 120.18 ug/g. 87–16 samples ranged from 87.29 to 160.74 ug/g with an average of 114.42 ug/g.) and heavy rare earth elements (HREE, 55-32 samples ranged from

TABLE 2 Major element concentrations (wt%), CIA, CIW, and ratio values of the investigated siliciclastic samples.

	Sample No	SiO_2 %	TiO_2 %	Al_2O_3 %	Fe_2O_3 tot%	MnO %	MgO %	CaO %	Na_2O %	K_2O %	P_2O_5 %	LOI %	Total	CIA	PIA	ICV	CIW	CaO^*	Al_2O_3/SiO_2	K_2O/Na_2O	Al_2O_3/TiO_2	DF1	DF2
High silica	S1	72.06	0.34	11.49	4.10	0.03	1.49	0.94	1.43	3.19	0.07	4.86	99.99	68.35	79.57	1.00	84.35	0.70	0.16	2.23	33.79	−4.44	−1.56
	S2	68.91	1.29	12.55	3.40	0.09	1.59	1.20	1.35	2.83	0.12	6.58	99.91	71.59	81.89	0.93	85.37	0.80	0.18	2.10	9.73	−5.60	−1.52
	S3	71.84	0.50	12.06	2.54	0.03	1.47	0.87	1.46	3.05	0.09	6.02	99.94	70.38	81.64	0.82	85.61	0.57	0.17	2.09	24.17	−5.38	−1.22
	S4	71.37	0.48	12.61	2.60	0.04	1.40	0.83	1.77	3.17	0.09	5.58	99.94	69.70	80.33	0.81	84.51	0.54	0.18	1.79	26.55	−4.87	−0.52
	S5	72.31	0.33	12.51	2.55	0.03	1.09	0.95	2.46	3.16	0.09	3.97	99.45	66.56	74.95	0.84	80.01	0.66	0.17	1.28	37.68	−3.81	0.83
	S6	71.73	0.75	12.46	2.72	0.06	1.10	1.10	2.38	3.11	0.09	4.43	99.93	66.44	74.60	0.90	79.65	0.80	0.17	1.31	16.57	−4.36	0.84
	S7	69.03	0.58	13.30	3.23	0.04	1.74	0.90	1.68	3.16	0.11	6.17	99.93	71.16	81.97	0.85	85.64	0.55	0.19	1.88	23.05	−4.65	−1.09
	S8	71.76	0.35	12.01	2.16	0.04	1.31	1.66	1.78	3.18	0.09	5.65	99.98	65.49	73.71	0.87	79.22	1.37	0.17	1.79	34.31	−4.71	−0.01
	S9	71.35	0.45	12.50	2.83	0.02	1.56	0.71	1.60	2.98	0.10	5.81	99.90	71.59	82.77	0.81	86.32	0.38	0.18	1.86	27.90	−4.88	−1.36
	S10	69.50	0.50	13.26	2.79	0.04	1.57	1.10	1.72	3.12	0.11	6.20	99.91	70.46	80.60	0.81	84.46	0.72	0.19	1.81	26.41	−4.43	−0.73
	S13	63.84	0.43	14.99	3.58	0.05	1.72	1.63	1.66	3.71	0.10	7.77	99.47	69.16	79.14	0.85	83.45	1.31	0.23	2.23	35.27	−3.30	−0.03
	S14	66.03	0.74	14.01	3.60	0.04	1.91	1.01	1.00	2.97	0.17	8.04	99.51	76.08	88.49	0.80	90.70	0.44	0.21	2.98	19.04	−4.53	−2.49
	S15	70.80	0.36	12.32	2.02	0.04	1.41	1.55	1.25	3.32	0.08	6.83	99.98	67.77	77.99	0.80	82.91	1.29	0.17	2.66	34.13	−5.30	−0.70
	S16	70.64	0.52	12.55	3.38	0.04	1.63	0.63	1.40	3.38	0.09	5.72	99.97	71.02	84.04	0.87	87.81	0.34	0.18	2.41	24.32	−5.30	−1.30
	S17	71.46	0.45	11.76	1.82	0.04	1.37	1.84	1.25	3.09	0.08	6.81	99.97	66.55	75.46	0.83	80.66	1.57	0.16	2.47	26.37	−5.43	−0.80
	S18	72.45	0.47	12.34	2.26	0.03	1.41	0.61	1.28	3.38	0.08	5.67	99.99	71.15	84.66	0.76	88.37	0.34	0.17	2.64	26.09	−5.94	−0.99
	S19	74.46	0.24	11.60	1.69	0.02	1.23	0.64	1.28	3.40	0.07	5.34	99.96	69.55	83.01	0.73	87.36	0.40	0.16	2.66	49.15	−6.15	−0.76
	S20	69.72	1.15	11.11	5.66	0.07	1.98	1.09	1.10	2.66	0.09	5.35	99.98	70.99	81.80	1.23	85.53	0.78	0.16	2.42	9.66	−5.08	−3.35
	S21	71.91	0.54	11.54	2.20	0.04	1.31	1.71	1.28	3.14	0.08	6.19	99.95	66.32	75.54	0.88	80.93	1.44	0.16	2.45	21.37	−5.47	−0.74
	S22	72.72	0.75	12.27	2.26	0.03	1.29	0.63	1.33	3.22	0.09	5.42	100.01	71.56	84.52	0.77	88.10	0.33	0.17	2.42	16.47	−6.06	−0.88
	S23	73.12	0.43	12.12	2.04	0.03	1.26	0.73	1.47	3.18	0.09	5.52	99.98	70.46	82.46	0.75	86.44	0.43	0.17	2.16	28.19	−5.53	−0.75
	S24	68.91	0.85	13.12	3.19	0.04	1.35	1.29	1.95	3.33	0.13	5.82	99.98	68.16	77.76	0.91	82.41	0.85	0.19	1.71	15.45	−4.52	0.29

(Continued on the following page)

10.3389/feart.2025.1573609

TABLE 2 (*Continued*) Major element concentrations (wt%), CIA, CIW, and ratio values of the investigated siliciclastic samples.

	Sample No	SiO_2 %	TiO_2 %	Al_2O_3 %	Fe_2O_3 %	MnO %	MgO %	CaO %	Na_2O %	K_2O %	P_2O_5 %	LOI %	Total	CIA	PIA	ICV	CIW	CaO*	Al_2O_3/SiO_2	K_2O/Na_2O	Al_2O_3/TiO_2	DF1	DF2
	S25	70.92	0.79	12.94	2.91	0.04	1.17	0.86	1.91	3.49	0.10	4.86	99.99	68.56	79.46	0.86	84.12	0.53	0.18	1.83	16.48	−4.94	0.50
	S26	72.53	0.41	12.83	2.16	0.02	1.13	0.65	1.98	3.31	0.08	4.88	99.98	69.40	80.21	0.75	84.53	0.37	0.18	1.67	31.22	−4.73	0.31
	S27	72.46	0.36	12.77	2.13	0.02	1.16	0.67	1.85	3.32	0.09	5.13	99.95	69.69	80.88	0.74	85.11	0.38	0.18	1.79	35.67	−4.81	0.09
	Average	70.87	0.56	12.52	2.79	0.04	1.43	1.03	1.58	3.19	0.09	5.78	99.90	69.52	80.30	0.85	84.54	0.72	0.18	2.11	25.96	−4.97	−0.72
	UCC[a]	66.62	0.64	15.4	5.04	0.1	2.48	3.59	3.27	2.8	0.15	--	--	62.70	66.46	1.16	70.77	3.09	0.23	0.86	24.06	−0.32	0.80
Low silica	Sample No	SiO_2%	TiO_2%	Al_2O_3%	Fe_2O_3 tot%	MnO%	MgO%	CaO%	Na_2O%	K_2O%	P_2O_5%	LOI%	Total	CIA	PIA	ICV	CIW	CaO*	Al_2O_3/SiO_2	K_2O/Na_2O	Al_2O_3/TiO_2	DF1	DF2
	S11	60.00	0.68	14.30	6.89	0.05	2.36	0.78	1.56	2.95	0.14	10.25	99.95	74.78	85.84	1.06	88.42	0.31	0.24	1.89	21.19	−2.25	−3.13
	S12	62.50	0.58	14.01	6.63	0.06	2.12	1.59	1.73	3.11	0.13	7.00	99.46	70.01	79.04	1.12	82.90	1.16	0.22	1.80	24.11	−1.70	−2.02
	Average	61.25	0.63	14.16	6.76	0.06	2.24	1.18	1.65	3.03	0.13	8.63	99.71	72.40	82.44	1.09	85.66	0.74	0.23	1.84	22.65	−1.98	−2.57
	UCC[a]	66.62	0.64	15.4	5.04	0.1	2.48	3.59	3.27	2.8	0.15	—	—	62.70	66.46	1.16	70.77	3.09	0.23	0.86	24.06	−0.32	0.80

CaO*(CaO from silicate fraction) = CaO − (10/3) × P_2O_5 (McLennan et al., 1993).
UCC[a]: average Upper Continental Crust (Rudnick and Gao, 2003).

10.3389/feart.2025.1573609

TABLE 3 Concentrations of selected trace elements (ppm) and ratios of the analysed samples.

Sample no.	Ba	Co.	Cr	Cu	Ga	Hf	La	Nb	Ni	Pb	Rb	Sc	Sr	Th	U	V	Y	Zn	Zr	La/Th	Cr/Th	Th/Sc	Cr/V	Y/Ni	Zr/Sc	Th*10	Zr/10	La/Y	Sc/Cr
S1	1,003.00	9.43	31.40	4.73	13.10	1.42	20.00	6.99	12.50	12.40	84.30	5.46	279.00	3.67	10.70	55.00	9.71	37.90	40.90	5.45	8.56	0.67	0.57	0.78	7.49	36.70	4.09	2.06	0.17
S2	1,024.00	5.80	42.60	6.13	13.00	1.33	27.40	8.71	10.50	13.60	77.20	7.29	367.00	6.26	3.31	58.40	11.50	40.00	43.60	4.38	6.81	0.86	0.73	1.10	5.98	62.60	4.36	2.38	0.17
S3	1,025.00	8.31	40.10	7.68	13.30	1.14	26.50	8.91	12.90	11.60	74.00	7.18	355.00	5.51	2.33	47.20	9.27	46.10	34.30	4.81	7.28	0.77	0.85	0.72	4.78	55.10	3.43	2.86	0.18
S4	1,052.00	6.95	43.10	12.20	15.00	1.35	33.70	9.59	12.70	14.30	85.10	7.60	359.00	12.50	13.80	89.00	8.61	51.30	44.00	2.70	3.45	1.64	0.48	0.68	5.79	125.00	4.40	3.91	0.18
S5	1,031.00	4.83	35.40	6.98	13.60	1.04	21.20	6.34	8.50	14.40	72.90	6.87	291.00	3.65	21.50	42.00	7.16	59.40	33.20	5.81	9.70	0.53	0.84	0.84	4.83	36.50	3.32	2.96	0.19
S6	1,005.00	5.37	44.00	7.83	13.50	1.14	29.00	11.90	8.80	11.60	74.50	8.15	325.00	6.00	17.70	70.50	11.20	52.90	38.50	4.83	7.33	0.74	0.62	1.27	4.72	60.00	3.85	2.59	0.19
S7	994.00	10.20	56.70	12.90	15.00	1.14	22.70	10.80	17.50	13.40	79.90	8.94	314.00	4.22	13.50	101.00	11.60	50.00	36.70	5.38	13.44	0.47	0.56	0.66	4.11	42.20	3.67	1.96	0.16
S8	1,123.00	5.69	30.10	8.32	12.80	1.25	22.50	6.58	10.90	10.80	73.00	5.79	310.00	3.79	2.91	143.00	7.58	34.00	41.40	5.94	7.94	0.65	0.21	0.70	7.15	37.90	4.14	2.97	0.19
S9	1,030.00	6.10	40.20	6.93	13.00	1.12	22.90	8.13	11.70	10.90	66.60	7.10	315.00	3.67	5.35	68.40	7.52	36.80	35.60	6.24	10.95	0.52	0.59	0.64	5.01	36.70	3.56	3.05	0.18
S10	1,003.00	14.30	51.00	17.50	14.70	1.47	27.00	9.36	18.40	14.10	80.00	8.61	316.00	4.94	15.00	209.00	9.32	52.80	51.10	5.47	10.32	0.57	0.24	0.51	5.93	49.40	5.11	2.90	0.17
S11	913.00	14.90	117.00	21.60	18.60	2.03	41.20	13.00	26.10	17.80	86.50	13.60	274.00	7.99	27.50	158.00	10.60	78.90	76.20	5.16	14.64	0.59	0.74	0.41	5.60	79.90	7.62	3.89	0.12
S12	1,014.00	14.30	68.30	16.00	17.50	1.38	35.10	10.80	24.70	14.10	87.10	11.90	303.00	5.07	32.20	74.10	7.61	54.40	44.30	6.92	13.47	0.43	0.92	0.31	3.72	50.70	4.43	4.61	0.17
S13	909.00	7.66	39.20	8.53	20.60	4.95	62.60	19.10	14.70	14.70	89.20	8.04	305.00	8.86	3.87	52.80	21.10	72.20	131.00	7.07	4.42	1.10	0.74	1.44	16.29	88.60	13.10	2.97	0.21
S14	933.00	13.20	71.20	13.80	17.30	2.67	44.30	16.10	20.60	18.10	85.90	11.20	365.00	7.00	1.91	75.20	19.90	70.40	96.30	6.33	10.17	0.63	0.95	0.97	8.60	70.00	9.63	2.23	0.16
S15	1,017.00	6.17	35.90	5.15	14.60	1.00	27.10	10.20	11.40	25.80	92.00	7.72	331.00	4.71	2.19	215.00	8.70	37.80	30.50	5.75	7.62	0.61	0.17	0.76	3.95	47.10	3.05	3.11	0.22
S16	1,023.00	6.37	43.10	12.20	14.70	1.33	22.30	11.30	12.20	11.80	82.40	7.10	302.00	5.64	1.86	178.00	7.60	42.90	43.20	3.95	7.64	0.79	0.24	0.62	6.08	56.40	4.32	2.93	0.16
S17	987.00	5.54	34.80	4.51	11.80	0.97	25.70	9.25	9.84	10.10	71.20	6.38	312.00	3.93	1.35	70.40	10.30	30.50	30.40	6.54	8.85	0.62	0.49	1.05	4.76	39.30	3.04	2.50	0.18
S18	1,057.00	7.24	39.40	4.26	13.90	1.39	28.10	10.40	12.10	11.70	86.30	7.50	320.00	5.18	1.62	123.00	8.35	34.50	45.10	5.42	7.61	0.69	0.32	0.69	6.01	51.80	4.51	3.37	0.19
S19	1,099.00	5.56	26.00	2.71	11.80	1.03	24.30	5.73	9.02	10.70	79.50	5.14	304.00	3.26	0.92	52.30	6.61	23.50	33.90	7.45	7.98	0.63	0.50	0.73	6.60	32.60	3.39	3.68	0.20
S20	840.00	13.40	51.20	7.93	15.00	2.17	39.20	19.90	14.50	10.80	66.30	9.35	230.00	9.01	4.60	207.00	12.60	39.30	72.80	4.35	5.68	0.96	0.25	0.87	7.79	90.10	7.28	3.11	0.18

(Continued on the following page)

10.3389/feart.2025.1573609

TABLE 3 (*Continued*) Concentrations of selected trace elements (ppm) and ratios of the analysed samples.

Sample no.	Ba	Co.	Cr	Cu	Ga	Hf	La	Nb	Ni	Pb	Rb	Sc	Sr	Th	U	V	Y	Zn	Zr	La/Th	Cr/Th	Th/Sc	Cr/V	Y/Ni	Zr/Sc	Th*10	Zr/10	La/Y	Sc/Cr
S21	924.00	5.89	37.90	5.29	12.10	1.25	25.90	10.20	10.50	10.90	75.80	6.68	278.00	4.73	1.69	179.00	12.30	30.70	39.90	5.48	8.01	0.71	0.21	1.17	5.97	47.30	3.99	2.11	0.18
S22	1,010.00	7.65	44.10	5.16	13.30	1.45	33.40	14.20	12.10	14.20	80.90	7.80	288.00	5.13	3.05	143.00	8.68	37.60	47.00	6.51	8.60	0.66	0.31	0.72	6.03	51.30	4.70	3.85	0.18
S23	1,014.00	6.83	35.40	6.47	13.10	1.07	27.20	7.94	10.70	11.60	77.50	6.81	297.00	3.37	1.84	97.00	7.48	32.60	33.80	8.07	10.50	0.49	0.36	0.70	4.96	33.70	3.38	3.64	0.19
S24	925.00	7.22	56.70	11.40	15.70	3.09	37.70	18.60	13.20	12.40	88.40	9.36	283.00	8.54	18.70	66.60	10.90	63.90	106.00	4.41	6.64	0.91	0.85	0.83	11.32	85.40	10.60	3.46	0.17
S25	951.00	6.97	48.50	9.05	16.10	2.05	40.40	19.20	12.30	14.80	99.40	8.94	274.00	9.02	21.20	57.00	11.60	36.50	64.80	4.48	5.38	1.01	0.85	0.94	7.25	90.20	6.48	3.48	0.18
S26	929.00	6.22	38.30	8.48	14.20	1.20	26.70	10.10	10.70	14.10	82.50	7.41	265.00	5.34	17.30	45.90	7.82	41.40	38.00	5.00	7.17	0.72	0.83	0.73	5.13	53.40	3.80	3.41	0.19
S27	1,022.00	6.77	35.50	7.39	14.50	1.25	23.80	8.34	11.30	12.90	87.10	7.27	279.00	4.19	16.30	43.60	7.27	30.60	36.60	5.68	8.47	0.58	0.81	0.64	5.03	41.90	3.66	3.27	0.20
Average	994.70	8.11	45.82	8.93	14.51	1.58	30.29	11.17	13.35	13.47	80.94	7.97	305.22	5.75	9.79	100.79	10.11	45.14	50.71	5.54	8.47	0.72	0.57	0.79	6.33	57.47	5.07	3.08	0.18
UCC[a]	624.00	17.30	92.00	28.00	17.50	5.30	31.00	12.00	47.00	17.00	84.00	14.00	320.00	10.50	2.70	97.00	21.00	67.00	193.00	2.95	8.76	0.75	0.95	0.45	13.79	105.00	19.30	1.48	0.15
PAAS[b]	650.00	20.00	100.00	—	—	5.00	38.20	18.00	60.00	20.00	160.00	16.00	—	14.60	—	140.00	—	—	210.00	2.62	6.85	0.91	0.71	—	13.13	146.00	21.00	—	0.16

UCC[a]: average Upper Continental Crust (Rudnick and Gao, 2003).
PAAS[b]: average post-Archean Australian Shale (McLennan, 1989).

13.2 38.61 ug/g with an average of 19.89 ug/g.) indicated significant fractionation. Samples 87-16 range from 12.92 24.12ug/g, with an average of 17.64 ug/g.) was also characterised by significant fractionation. LREE/HREE (samples 55-32 range from 4.63 to 7.85, with an average of 6.12. Samples 87-16 range from4.37~7.36 with an average of 6.53), with fractionation factors higher than those of UCC and PAAS.

4.2.4 Geochemical weathering indices

The geochemical weathering index encompasses several key metrics, including the Alteration Chemical Index (CIA) developed by Nesbitt and Young (1982), the Alteration Plagioclase Index (PIA) introduced by Fedo et al. (1995), the Weathering Chemical Index (CIW) established by Harnois (1988), and the Composition Variation Index (ICV) proposed by Cox et al. (1995). These indices were derived from the primary oxide values present in the analyzed sediment, as detailed in the Methods section. The calculated values for CIA, PIA, CIW, and ICV are presented in Table 2.

5 Discussion

The contents of major element oxides, trace elements, and rare earth elements in clastic sedimentary rocks provide valuable information for understanding paleoenvironmental conditions during deposition. This method has been widely used to infer the depositional conditions of sedimentary formations (Moradi et al., 2016; Xie et al., 2018; Wei and Algeo, 2020; Fathy et al., 2021; Hussain et al., 2021; Yan et al., 2021; Al-Juboury et al., 2021; Omietimi, 2022; Tang et al., 2023; Zhang et al., 2023; Xiao et al., 2023; Yang et al., 2023; Qureshi et al., 2023). In this study, major element oxides, trace element and rare earth element compositions were used to assess palaeo-weathering and climate variability, palaeo-temperature, palaeo-productivity, salinity, hydro-energetic conditions and palaeo-oxidation levels in the Ordos Basin.

5.1 Provenance

5.1.1 Provenance from major elements

The elemental geochemistry, encompassing major, trace, and rare earth elements, of clastic sedimentary rocks has been utilized to deduce their provenance (McLennan et al., 1993; Roser and Korsch, 1986; Augustsson et al., 2023). Certain oxides, such as aluminum oxide (Al2O3) and titanium dioxide (TiO2), along with trace elements including scandium (Sc), nickel (Ni), lanthanum (La), cobalt (Co.), chromium (Cr), vanadium (V), niobium (Nb), hafnium (Hf), yttrium (Y), zirconium (Zr), and thorium (Th), exhibit low mobility or immobility throughout the processes of transportation, weathering, and diagenesis of their parent rocks (Hayashi et al., 1997; Cullers, 2000; Augustsson et al., 2023). The analysis of major, trace, and rare earth elements facilitated the identification of the source rock types present in the studied sandstones. This topic can be elaborated upon as follows:

The major oxides are insufficient for accurately determining the provenance of siliciclastic rocks, as many of these oxides are subject to mobility due to weathering and diagenetic processes

TABLE 4 Rare earth element concentrations (ppm) and ratios of analysed samples.

Sample no.	La	Ce	Pr	Nd	Sm	Eu	Gd	Tb	Dy	Ho	Er	Tm	Yb	Lu	Y	∑REEs	∑LREEs	∑HREEs	∑LREEs/∑HREEs	Eu/Eu*	Ce/Ce*	La/Yb	(La/Yb)cn	(La/Sm)cn	(Gd/Yb)cn
S1	20.00	37.30	4.41	16.20	2.67	1.13	2.28	0.36	1.78	0.34	0.96	0.17	1.09	0.15	9.71	98.55	81.71	16.84	4.85	1.28	0.90	18.35	10.45	4.71	1.69
S2	27.40	47.00	5.64	20.20	3.15	1.24	2.68	0.41	2.15	0.42	1.21	0.20	1.28	0.18	11.5	124.66	104.63	20.03	5.22	1.19	0.85	21.41	12.19	5.48	1.69
S3	26.50	45.00	5.57	20.20	3.17	1.24	2.70	0.40	1.98	0.35	1.07	0.17	1.10	0.16	9.27	118.89	101.68	17.21	5.91	1.18	0.83	24.09	13.72	5.26	1.98
S4	33.70	59.50	6.41	23.00	3.40	1.19	2.86	0.40	1.88	0.33	1.01	0.16	1.02	0.14	8.61	143.62	127.20	16.42	7.75	1.06	0.90	33.04	18.82	6.24	2.26
S5	21.20	37.80	4.33	15.90	2.45	1.09	2.14	0.32	1.51	0.28	0.77	0.12	0.78	0.12	7.16	95.97	82.77	13.20	6.27	1.33	0.88	27.11	15.44	5.45	2.21
S6	29.00	52.00	6.00	22.20	3.43	1.23	2.85	0.44	2.21	0.41	1.20	0.20	1.32	0.19	11.2	133.88	113.86	20.02	5.69	1.09	0.88	21.97	12.51	5.32	1.74
S7	22.70	43.00	5.23	20.00	3.33	1.19	2.69	0.44	2.29	0.44	1.28	0.22	1.45	0.20	11.6	116.07	95.45	20.62	4.63	1.10	0.90	15.66	8.92	4.29	1.50
S8	22.50	40.30	4.84	17.80	2.83	1.23	2.33	0.35	1.67	0.30	0.88	0.14	0.92	0.13	7.58	103.80	89.50	14.30	6.26	1.33	0.87	24.59	14.00	5.00	2.05
S9	22.90	41.80	4.94	18.40	3.00	1.12	2.39	0.36	1.75	0.30	0.87	0.14	0.94	0.13	7.52	106.57	92.16	14.41	6.40	1.16	0.89	24.26	13.81	4.80	2.04
S10	27.00	47.50	5.54	20.90	3.33	1.24	2.74	0.41	2.08	0.38	1.10	0.19	1.26	0.19	9.32	123.18	105.51	17.67	5.97	1.14	0.87	21.43	12.20	5.10	1.75
S11	41.20	63.10	6.69	23.80	3.45	1.10	3.18	0.46	2.24	0.41	1.17	0.20	1.24	0.19	10.6	159.03	139.34	19.69	7.08	0.93	0.82	33.23	18.92	7.52	2.07
S12	35.10	51.10	5.10	17.90	2.79	1.08	2.50	0.34	1.63	0.29	0.85	0.14	0.92	0.14	7.61	127.48	113.07	14.41	7.85	1.14	0.80	38.36	21.85	7.92	2.20
S13	62.60	119.00	12.10	43.90	7.06	1.72	5.97	0.88	4.30	0.80	2.31	0.38	2.50	0.37	21.1	284.99	246.38	38.61	6.38	0.74	0.96	25.04	14.26	5.58	1.93
S14	44.30	91.50	9.77	36.20	5.94	1.55	4.98	0.81	3.94	0.72	2.04	0.35	2.09	0.31	19.9	224.39	189.26	35.13	5.39	0.79	1.00	21.20	12.07	4.69	1.92
S15	27.10	44.80	5.29	19.80	3.11	1.11	2.67	0.39	1.84	0.32	0.99	0.15	0.94	0.13	8.7	117.34	101.21	16.13	6.27	1.07	0.83	28.98	16.51	5.48	2.30
S16	22.30	39.10	4.74	17.50	2.73	0.92	2.27	0.34	1.58	0.28	0.91	0.14	0.89	0.13	7.6	101.44	87.29	14.15	6.17	1.03	0.86	25.00	14.24	5.14	2.05
S17	25.70	43.20	5.16	19.10	3.01	1.09	2.55	0.39	2.03	0.37	1.20	0.19	1.10	0.16	10.3	115.54	97.26	18.28	5.32	1.10	0.84	23.36	13.31	5.37	1.87
S18	28.10	48.50	5.65	21.10	3.31	1.14	2.71	0.41	1.89	0.33	1.00	0.15	0.97	0.13	8.35	123.73	107.80	15.93	6.77	1.06	0.86	29.12	16.58	5.34	2.27
S19	24.30	40.70	4.87	18.00	2.88	1.13	2.38	0.36	1.59	0.26	0.78	0.11	0.73	0.10	6.61	104.80	91.88	12.92	7.11	1.20	0.84	33.33	18.98	5.31	2.63
S20	39.20	75.60	8.55	31.10	4.77	1.24	3.98	0.60	2.84	0.50	1.62	0.24	1.54	0.21	12.6	184.58	160.46	24.12	6.65	0.79	0.93	25.45	14.50	5.17	2.09
S21	25.90	41.50	5.16	18.80	3.02	1.01	2.66	0.44	2.37	0.47	1.55	0.25	1.58	0.22	12.3	117.23	95.39	21.84	4.37	0.99	0.80	16.39	9.34	5.40	1.36
S22	33.40	58.60	6.75	25.00	3.94	1.17	3.21	0.47	2.19	0.37	1.16	0.17	1.11	0.16	8.68	146.37	128.86	17.51	7.36	0.91	0.87	30.09	17.14	5.34	2.33

(Continued on the following page)

10.3389/feart.2025.1573609

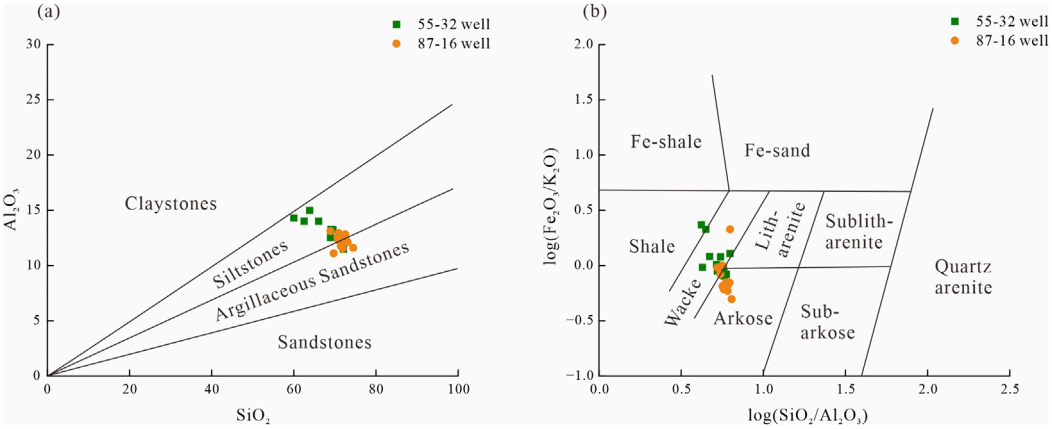

FIGURE 3
(a) Chemical classification of the sampled sedimentary rocks according to Sprague et al. (2009) and **(b)** according to Herron (1988).

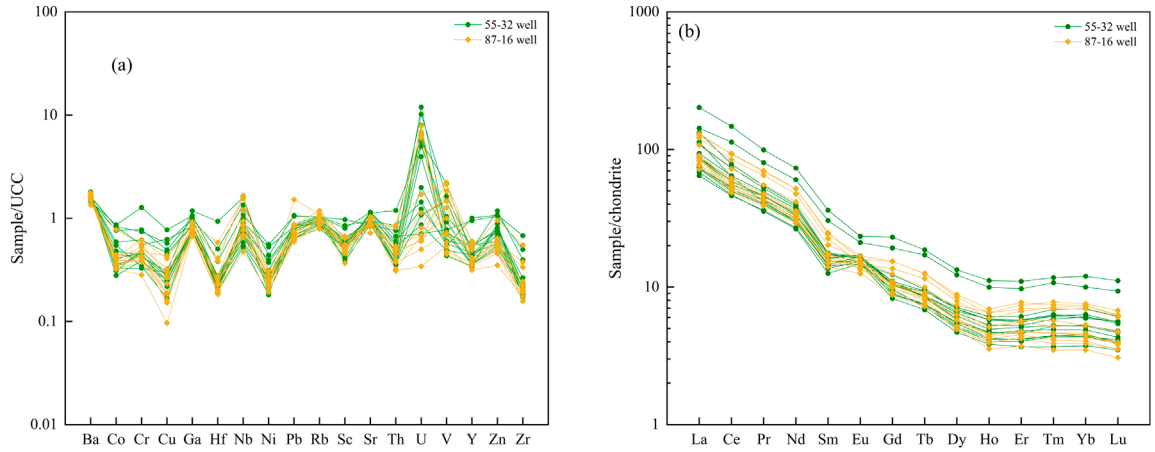

FIGURE 4
(a) Trace element variation diagram for all samples normalised to UCC (Rudnick and Gao, 2003). **(b)** Rare earth elements of all samples normalised to chondrite composition (Taylor and McLennan, 1985).

(Augustsson et al., 2023). Research indicates that the ratios of K_2O/Na_2O and Al_2O_3/TiO_2 serve as effective provenance indicators for terrestrial deposits (Hayashi et al., 1997; Roser and Korsch, 1986; Roser and Korsch, 1988; Hayashi et al., 1997; Augustsson et al., 2023). Hayashi et al. (1997) asserted that aluminum (Al) and titanium (Ti) are typically compatible and exhibit immobility during both pre-depositional and post-depositional processes. Augustsson et al. (2023) demonstrated that K_2O/Na_2O ratios are effective indicators for identifying the source rocks of sediments in arid climatic conditions and terrestrial depositional environments, as opposed to humid and marine settings. The ineffectiveness of K_2O/Na_2O as an indicator for sediments formed in terrestrial depositional environments characterized by humid climates may be attributed to the extensive weathering of K_2O/Na_2O under such climatic conditions (Augustsson et al., 2023). According to Hayashi et al. (1997), the Al_2O_3/TiO_2 ratios serve as indicators of the source rock type, with values between 3 and 8 suggesting mafic igneous origins, while ratios from 8 to 21 are indicative of intermediate igneous source rocks. Conversely, ratios ranging from 21 to 70 are associated with felsic igneous source rocks. In the analysis of the sandstone from the 55-32 well, the Al_2O_3/TiO_2 ratio was observed to range from 9.73 to 37.68, whereas the ratio for the sandstone from the 87-16 well varied from 9.66 to 49.15. These findings align closely with the characteristics of felsic and intermediate igneous provenances, as noted by Hayashi et al. (1997).

Roser and Korsch's (1988) discriminant function plots for the major oxides indicate that quartzose sedimentary provenance and felsic igneous rocks are the main sources of the studied sandstones (Figure 5a). In addition, plotting the bivariate diagrams (TiO_2 versus Al_2O_3 and TiO_2 versus Zr) of Hayashi et al. (1997) documented the felsic and intermediate igneous provenance for the studied sandstones (Figures 5b, c). The plot of Le Bas et al. (1986) for Al_2O_3/TiO_2 versus SiO_2 reflects a felsic source with a small contribution from an intermediate igneous source (Figure 5d). Therefore, the major element study shows that the sandstone of the

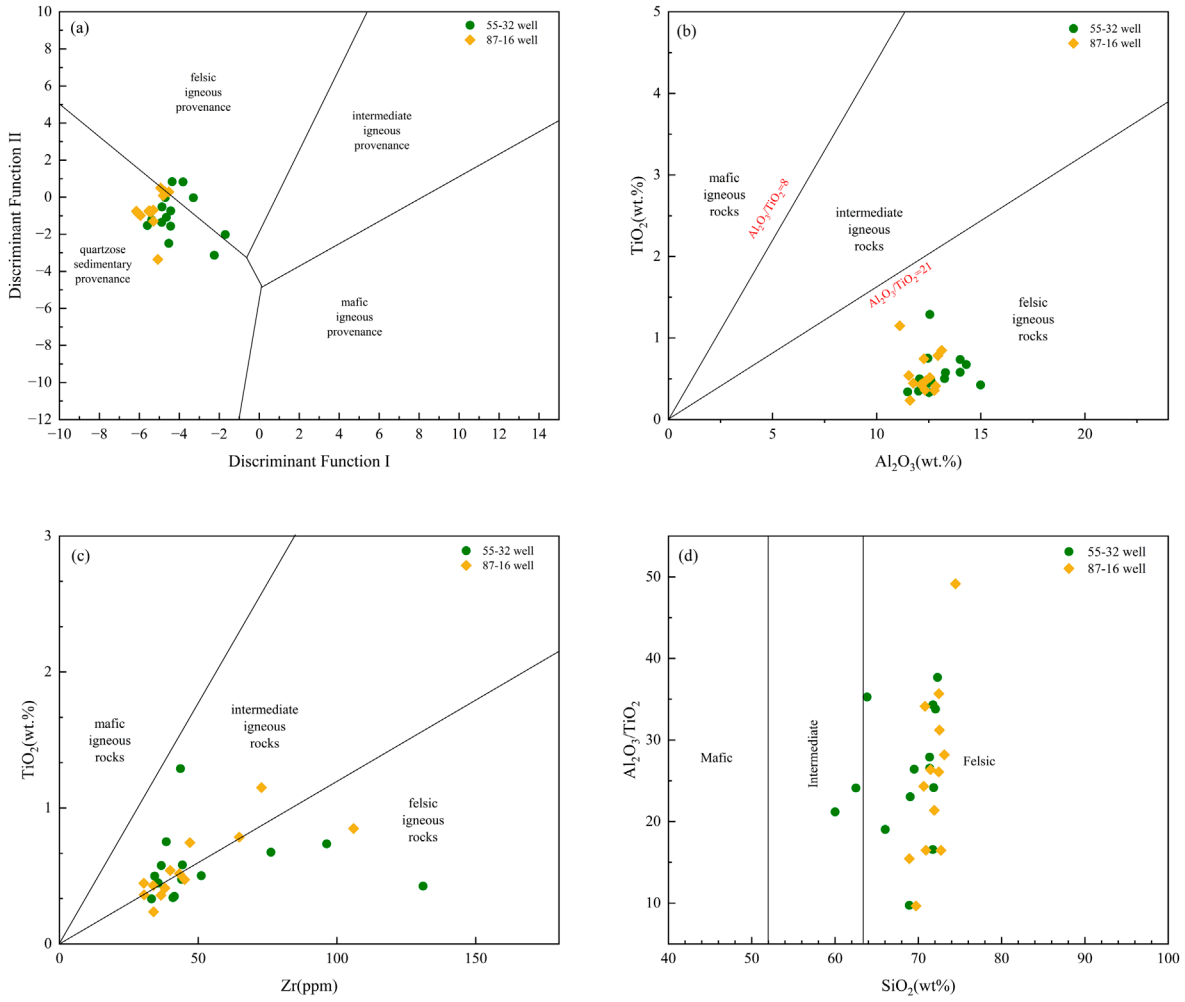

FIGURE 5
Provenance discriminant function diagrams using major elements **(a)** (after Roser and Korsch, 1988) and **(b, c)** Al_2O_3 versus TiO_2 and Zr (ppm) versus TiO_2 (wt%) (after Hayashi et al., 1997), and **(d)** Al_2O_3/TiO_2 versus SiO_2 (after Le Bas et al., 1986).

Zhiluo Formation is a feldspathic source rock formed by geological processes.

5.1.2 Provenance from trace elements

The use of trace elements, including titanium (Ti), thorium (Th), scandium (Sc), niobium (Nb), yttrium (Y), hafnium (Hf), and zirconium (Zr), is essential for determining the provenance of clastic sedimentary rocks. Their natural compatibility and stability during recycling and diagenesis processes greatly enhance their value as dependable indicators for inferring the origins of these geological formations (Floyd and Leveridge, 1987; McLennan et al., 1993; Cullers, 2000; Totten et al., 2000; Hiscott, 1984; Bracciali et al., 2007; Augustsson et al., 2023).

In the sandstones of the 55–32 well, a notable depletion was observed in the contents of Sc, Co., Ni, Cu, La, Ga, and Zn, with average values of 8.41, 9.07, 15.04, 10.95, 31.15, 15.07, and 52.65 ppm, respectively (refer to Table 3). Similarly, the 87-16 well sandstones exhibited a depletion in these trace elements, with average values of 7.49, 7.06, 11.53, 6.92, 29.37, 13.91, and 37.06 ppm (also see Table 3). The normalized pattern of these trace elements was analyzed in relation to the Upper Continental Crust (UCC) (Taylor and McLennan, 1985). The analysis indicated that the examined sandstones exhibited a slight enrichment in barium (Ba), rubidium (Rb), vanadium (V), and uranium (U), while showing a depletion in cobalt (Co.), chromium (Cr), copper (Cu), nickel (Ni), yttrium (Y), and zirconium (Zr) when compared to the upper continental crust (UCC) (Figure 4). The other trace elements found in the examined sandstones closely resembled the normalization values (Figure 4). The data suggest that the studied sandstones originate from a felsic igneous source (McLennan et al., 1993; Löwen et al., 2018). The trace element values of the analyzed sandstones are presented in bivariate diagrams, including Hf versus La/Th (Floyd and Leveridge, 1987), Co./Th versus La/Sc (McLennan et al., 1993), Th/Sc versus Cr/Th (Totten et al., 2000), and Cr/V versus Y/Ni (McLennan et al., 1993), labeled as diagrams a, b, c, and d, respectively. Also, presentation of the studied samples on the Ni–V–Th*10 ternary diagram of Bracciali et al. (2007) (Figure 6a) and Ni versus TiO_2 and Th/CO versus La/Sc

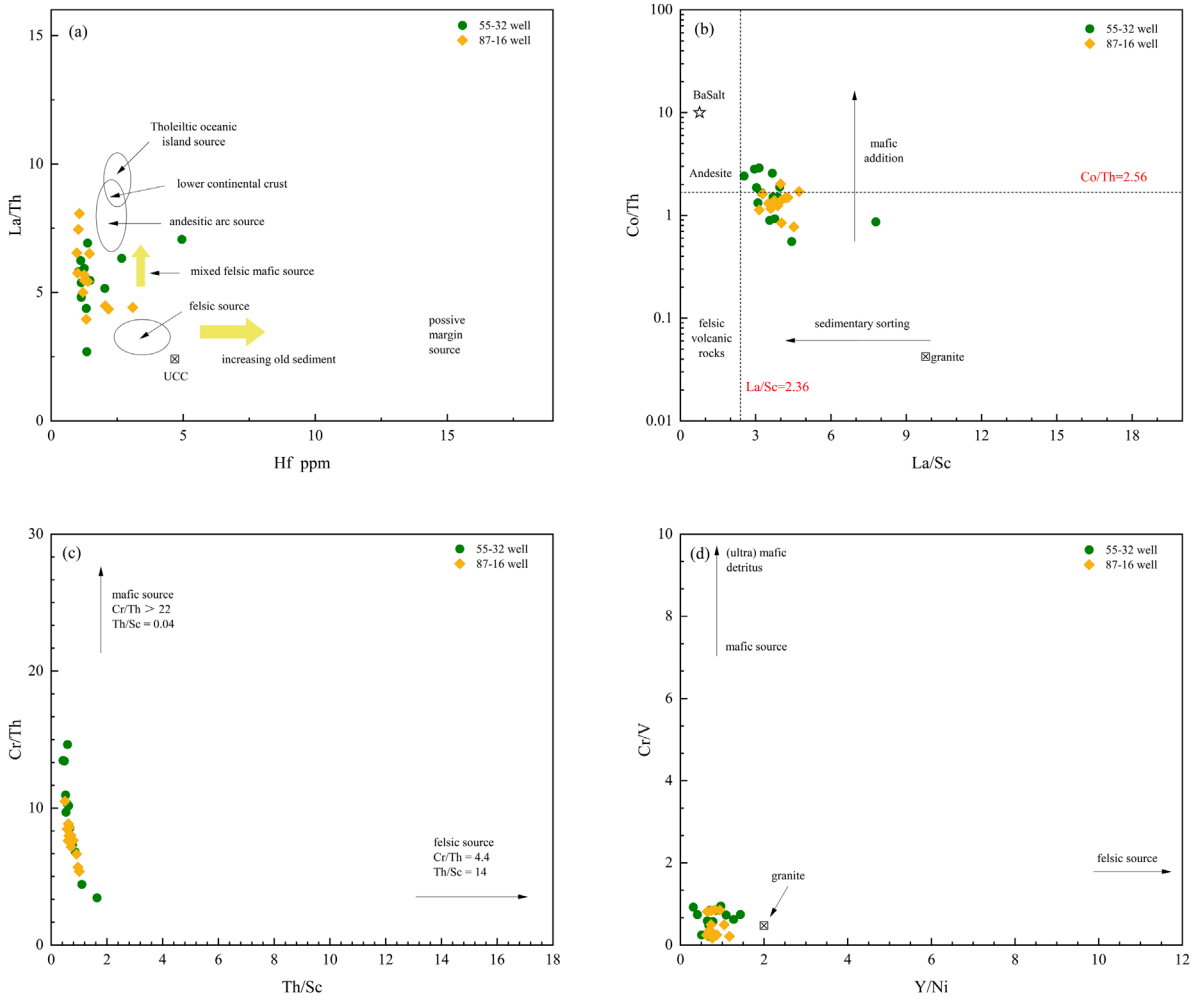

FIGURE 6
(a–d) Plot provenance determination of the analysed sandstone samples on the Ni–V–Th*10 ternary diagram after Bracciali et al. (2007), the Ni/TiO_2 bivariate diagram of Floyd and Leveridge (1987), the Th/Co. versus La/Sc diagram of Cullers (2000), and the Th/Sc versus Zr/Sc diagram of McLennan et al. (1993).

binary diagrams (Figures 6b, c) showed that the studied samples approached the felsic field rather than the mafic field.

The findings suggest a significant contribution from a felsic igneous source, with only a minor input from a mafic igneous source in the analyzed samples. The low Cr/V ratios, when compared to the Y/Ni ratios (as shown in Table 3), indicate a felsic origin for the sediments under study, effectively ruling out the likelihood of contributions from mafic or ultramafic sources (McLennan et al., 1993).

5.1.3 Provenance from rare earth elements

Due to their limited mobility and significant stability throughout weathering, transportation, and diagenetic processes of the parent rocks (Taylor and McLennan, 1985), rare earth elements (REEs) serve as valuable indicators for identifying the type of parent rocks from which clastic rocks originate. The distribution pattern of rare earth elements (REEs) and europium anomalies in clastic sediments offers compelling evidence for determining the composition of source rocks (Taylor and McLennan, 1985; Cullers, 1994; Rudnick and Gao, 2003; Armstrong-Altrin et al., 2015), the high ratios of light rare earth elements (LREE) to heavy rare earth elements (HREE) and the presence of negative europium (Eu) anomalies in clastic rocks suggest a felsic source. In contrast, the lower LREE/HREE ratios and the absence of Eu anomalies in clastic rocks indicate a mafic source (Cullers, 1994). Utilizing the REE values identified in the analyzed sandstones is essential for determining their source rocks.

In these sandstones, the elevated levels of LREE (55–32 well, average 120.18; 87-16 well, average 114.42) compared to the HREEs (averages of 19.89 and 17.64) as shown in Table 4, indicate a felsic igneous source (Cullers, 1994). The elevated average ratios of (La/Yb) cn, recorded at 14.23 and 15.55, alongside the lower averages of (Gd/Yb) cn, which are 1.93 and 2.21, in the analyzed rocks (refer to Table 4), imply a granitic origin for the source rocks (Rudnick and Gao, 2003). The sandstone samples examined exhibit higher LREE/HREE values, ranging from 4.37 to 7.85, with an average of 6.32, and display negative Eu anomalies between 0.92 and 1.72, averaging at 1.17. Conversely, a subset of these

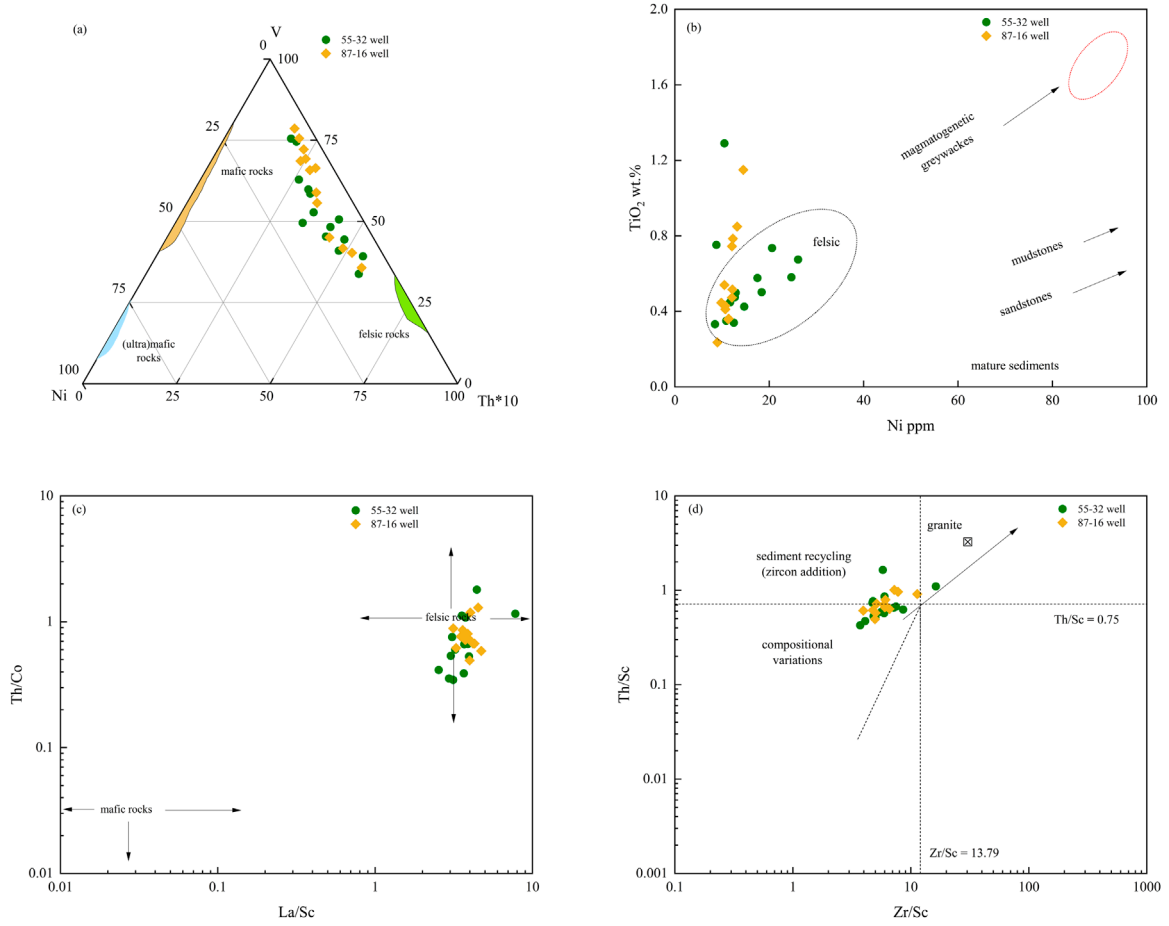

FIGURE 7
(a–d) Bivariate plots of provenance-diagrams using trace elements of the studied sandstones (after Floyd and Leveridge, 1987; McLennan et al., 1993; Totten et al., 2000; McLennan et al., 1993, respectively).

samples shows lower LREE/HREE values, between 2.40 and 2.90, accompanied by minimal negative Eu anomalies ranging from 0.30 to 4.02 (see Table 4). The presence of higher LREE/HREE ratios coupled with negative Eu anomalies further supports the conclusion of a granitic source for the Upper Continental Crust (UCC) (Taylor and McLennan, 1985; Rudnick and Gao, 2003). Conversely, the lower LREE/HREE values, along with the presence of minimal negative anomalies, suggest that mafic source rocks significantly contribute to the composition of the studied sandstones (Cullers, 1994). The observed relative enrichment of light rare earth elements (REE) and a low Eu/Eu* ratio (average of 1.04) as indicated in Table 4 suggest that the studied sandstones originate from a granitic source associated with the Upper Continental Crust (UCC) (Amedjoe et al., 2018) (Figure 7).

In conclusion, the analysis of major, trace, and rare earth elements suggests that the detrital sources of the studied sandstone are diverse. This mixed source comprises fragments of felsic, medium, and mafic igneous rocks. The Changying igneous rocks are likely derived from granite and volcanic formations, specifically rhyolite. The moderate igneous contribution can be attributed to a combination of intrusive rocks, such as granodiorite, and extrusive rocks like andesite. Furthermore, the provenance of mafic igneous rocks in this study may be linked to volcanic rocks, particularly basalt, found in the northern region of the Ordos Basin. Additionally, the sedimentary origin of quartzite may be associated with multi-cyclic acidic rocks, including granite.

5.2 Tectonic setting of the source area

The original mineralogy and geochemistry of clastic sedimentary rocks can undergo changes due to diagenesis (Pettijohn et al., 1987). Additionally, the heavy mineral assemblage (Nechaev, V.P., 1993) and elemental geochemistry, including major, trace, and rare earth elements (Bhatia, 1983; Roser and Korsch, 1986; Verma and Armstrong-Altrin, 2013), have been extensively utilized to infer the tectonic setting of their source areas. This topic will be further explored in the following discussion.

5.2.1 Tectonic setting from major elements

Numerous prior studies have demonstrated that the primary components of siliciclastic sedimentary rocks can effectively

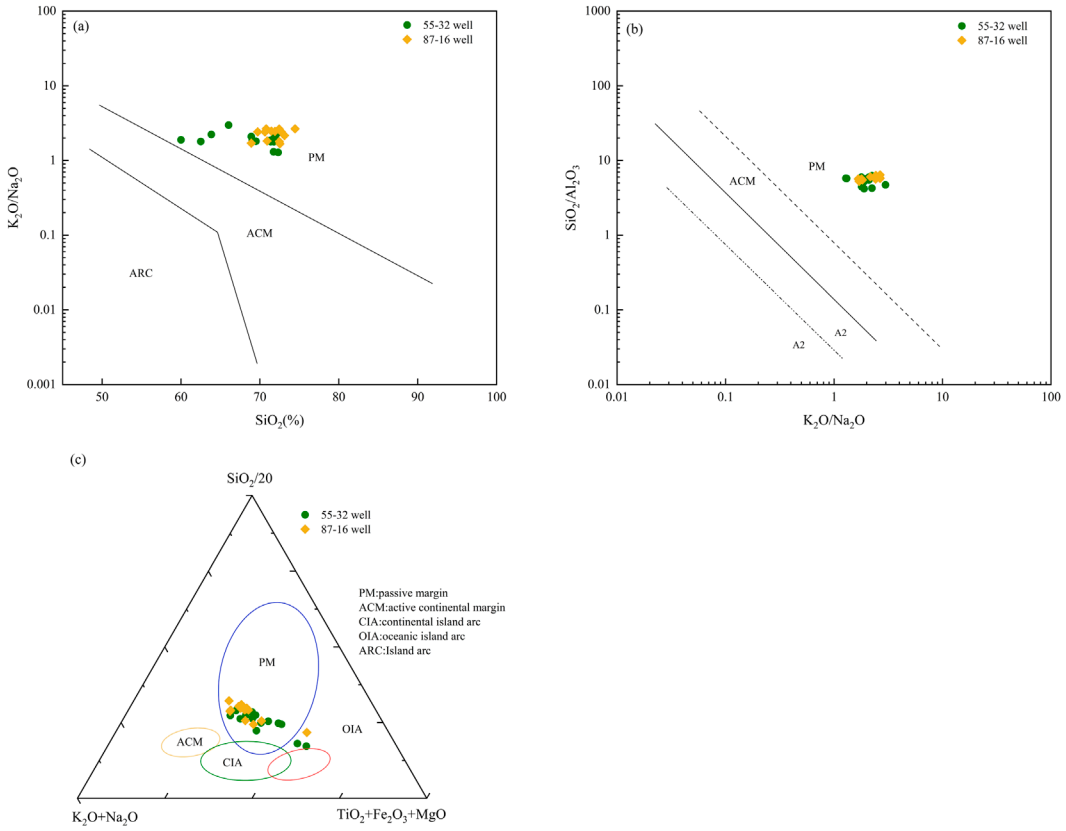

FIGURE 8
Plots of major elements of the studied sandstones on the tectonic discrimination diagrams of **(a, b)** Roser and Korsch (1986), **(c)** Kroonenberg (1994). Note: PM = passive margin; ACM = active continental margin; CA = continental island-arc.

differentiate the tectonic settings of their source rocks (Bhatia, 1983; Roser and Korsch, 1986; Verma and Armstrong-Altrin, 2013; Verma and Armstrong-Altrin, 2016). The representation of the discriminant functions of major oxides from the analyzed sandstones in the diagrams by Bhatia (1983), Roser and Korsch (1986), and Kroonenberg (1994) indicates a passive continental margin setting for their source rocks (Figures 8a–c). Furthermore, the application of the new discriminant function diagrams by Verma and Armstrong-Altrin (2016) reinforces this conclusion of a passive margin setting (Figures 9a, b).

5.2.2 Tectonic setting from trace and rare earth elements

The stability of trace and rare earth elements during the weathering and diagenesis of the parent rock (Taylor and McLennan, 1985) is crucial. Additionally, the presence of these elements in clastic sedimentary rocks significantly influences the identification of the tectonic settings of the source rocks (Bhatia and Crook, 1986; McLennan et al., 1993; McLennan, 2001). The analysis of trace element values from the studied rocks, as illustrated in the diagrams by Bhatia and Crook (1986), indicates that the samples predominantly align with or are situated near the continental island-arc field (Figures 10a–c). The analyzed sandstones originated from weathered rocks in a continental island-arc environment. Additionally, the striking similarities in the rare earth element (REE) distribution between the studied samples and the average normalization of those from the Upper Continental Crust (UCC) and Post-Archean Australian Shale (PAAS), along with the presence of negative europium anomalies (Figure 4b), indicate that their source rocks were likely derived from a passive continental margin setting (Taylor and McLennan, 1985; McLennan, 1989). The analysis indicates a significant enrichment of light rare earth elements (REEs), with an average concentration of 117 μg/g. Additionally, the low Eu/Eu^* ratio, which is less than 0.94, along with the nearly flat chondrite-normalized patterns of heavy REEs, suggests that the studied sandstones originate from a granitic source within the Upper Continental Crust (UCC) (Amedjoe et al., 2018).

5.3 Source area-paleoweathering

Chemical weathering induces alterations in the mineralogical and chemical compositions of the parent rocks (Pettijohn et al., 1987). Consequently, an examination of the mineralogical and chemical characteristics of clastic sedimentary rocks can provide valuable insights into the impact of chemical weathering on their source areas.

The significant reduction of CaO, Na_2O, and K_2O (the alkaline elements) in the analyzed samples, in comparison to the Upper Continental Crust (UCC) values (refer to Table 2), can be attributed

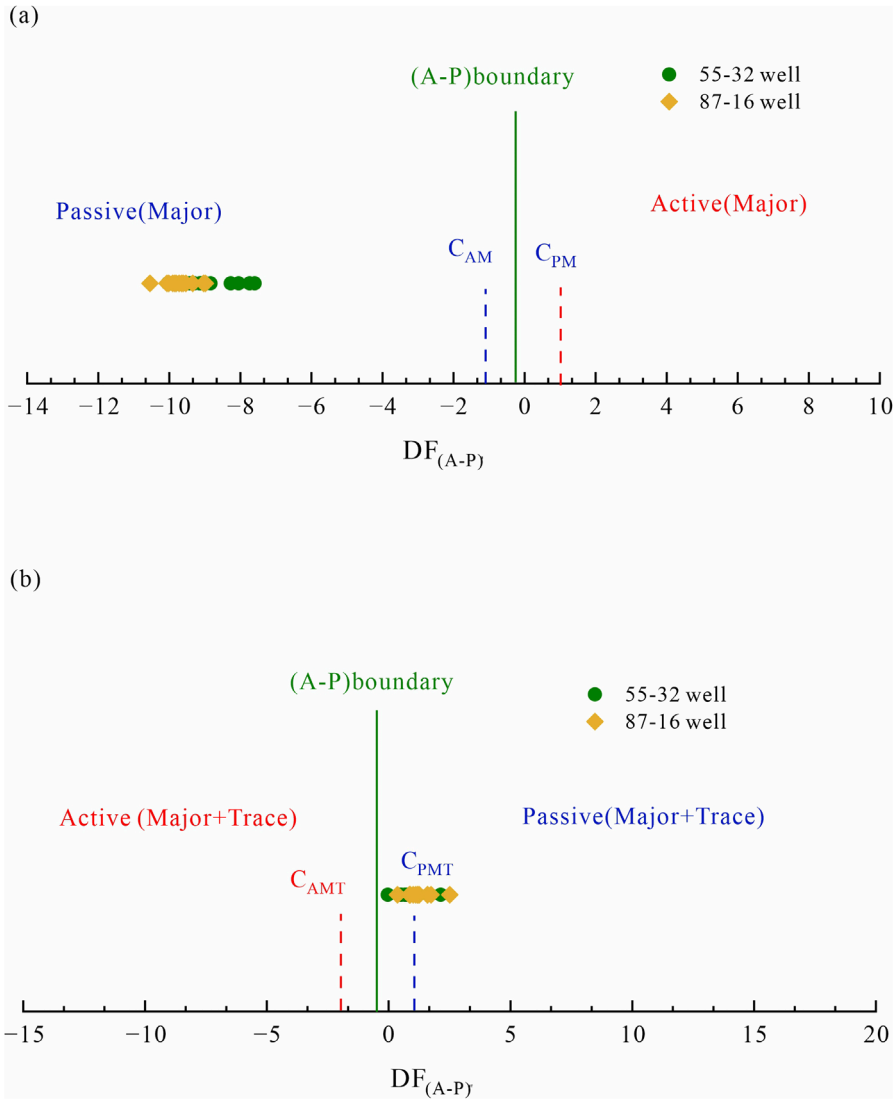

FIGURE 9
Tectonic setting of the studied sandstones using diagrams of Verma and Armstrong-Altrin (2016) for **(a)** major elements, **(b)** combined major and trace elements.

to the enhanced mobility of these elements during moderate to intense chemical weathering (Gaillardet et al., 1999). The elevated SiO_2/Al_2O_3 ratios presented in Table 2 suggest a significant level of chemical maturity and indicate that the studied sediments have undergone multiple cycles of recycling (Roser and Korsch, 1986). The geochemical indices, including CIA, CIW, PIA, and ICV, indicate that the CIA values of the studied samples range from 65.48% to 76.07%, with an average of 69.73%. This suggests a moderate to high degree of chemical weathering affecting their source rocks (Nesbitt and Young, 1982). The values of the CIW, which range from 79.22% to 90.70%, indicate significant alteration of feldspars in the granitic igneous rocks, as shown in Table 2 (Fedo et al., 1995). The values of the PIA for the studied samples, which range from 73.71% to 88.49% (as shown in Table 2), indicate a significant alteration of plagioclase and K-feldspar in the source rocks (Harnois, 1988). The values of the ICV for the studied samples are predominantly less than 1, with the exception of three samples (refer to Table 2). This indicates that the source rocks have undergone significant chemical weathering (Cox et al., 1995; Cullers, 2000). The analysis of the studied sandstones indicates that the intensive chemical weathering and recycling of their source rocks is supported by a comparison of the CIA values with A–CN–K, as illustrated in the diagram by Long et al. (2012) (Figure 11a) and ternary diagram of Al_2O_3, Ti_2O and Zr in the studied sandstones (Figure 11b) of Garcia et al. (1991). This intensive chemical weathering is also documented using the binary diagram of CIA versus ICV of Nesbitt and Young (1982) (Figure 11c). The analysis of trace elements provides insights into the intensity of chemical weathering on source rocks. The low average Th/Sc ratio of 0.72, coupled with a high Th/U ratio of 1.47 (as shown in Table 3), indicates that the source rocks have undergone significant chemical weathering (McLennan et al., 1993). The analyzed sandstones

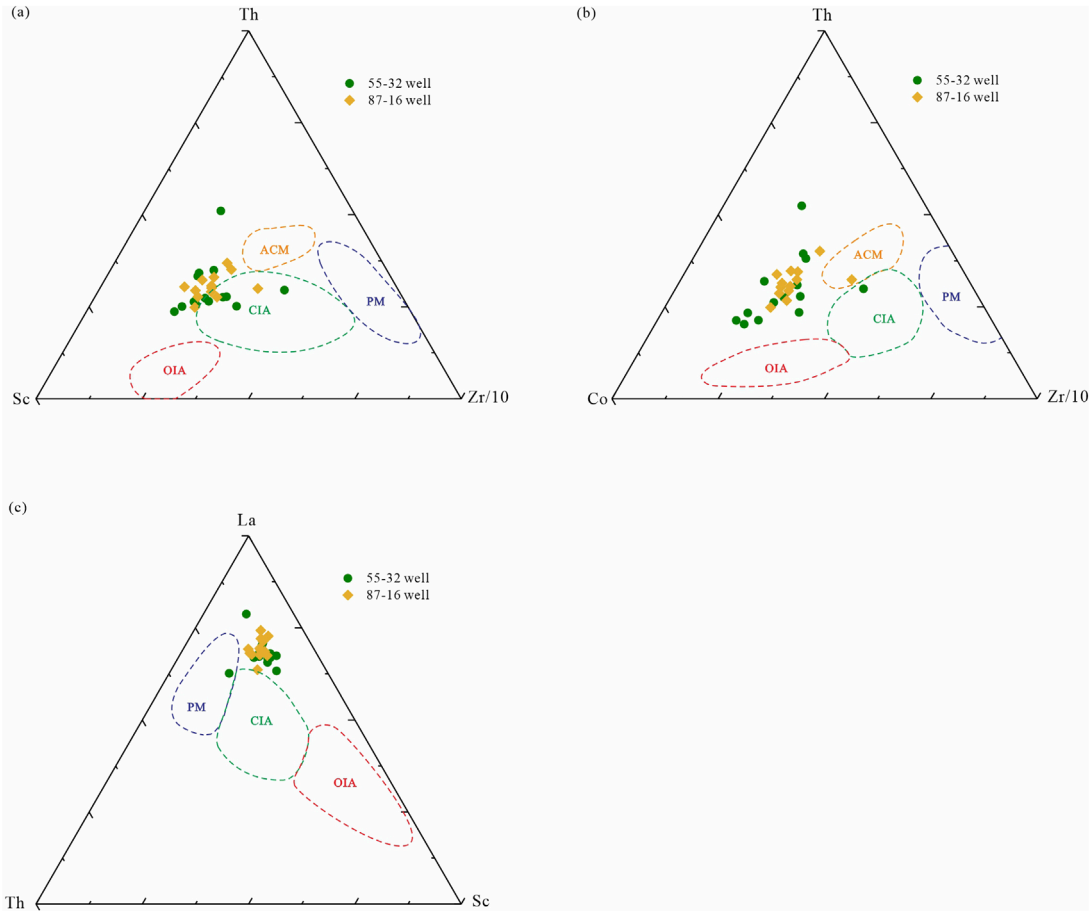

FIGURE 10
Plots of trace elements of the studied sandstones on the tectonic discrimination diagrams of Bhatia and Crook (1986) for: **(a)** Th–Sc–Zr/10 ternary diagram, **(b)** Th–Co–Zr/10 ternary diagram, and **(c)** La–Th–Sc ternary diagram. Notice, PM = passive margin, ACM = active continental margin, CIA = continental island-arc.

exhibit elevated Th/U ratios, averaging 1.47, which suggests a dominance of oxidizing conditions during chemical weathering, as noted by Taylor and McLennan (1985). When the Th and U data from these sandstones are plotted on the binary diagram (Th/U versus Th) presented by McLennan et al. (1993), it highlights the significant impact of intense chemical weathering and recycling on the source rocks.

5.4 Paleoclimate analysis

5.4.1 Paleosalinity

Paleosalinity offers insights into ancient sedimentary environments by distinguishing different types of sedimentary water and indicating the water depth at the time of sediment deposition (Yang et al., 2023). Geochemical analyses can effectively evaluate the paleosalinity of sedimentary deposits found in freshwater, brackish, and deep marine environments (Omietimi et al., 2022; Zhang et al., 2023; Yang et al., 2023; Qureshi et al., 2023). Insights into paleosalinity conditions can be derived by examining the proportions of magnesium (Mg), aluminum (Al), calcium (Ca), and sodium (Na). The ratios of strontium to barium (Sr/Ba), 100 times the ratio of magnesium to aluminum (100*Mg/Al), and calcium to aluminum (Ca/Al) have proven to be valuable tools for comprehending variations in paleosalinity levels within sedimentary rock formations (Wei and Algeo, 2020; Chen et al., 2021; Wang et al., 2021; Yan et al., 2021; Omietimi, 2022). The correlation between strontium enrichment and rising paleo-water salinity is significant, as salinity levels typically increase with depth (Omietimi et al., 2022). Elevated Sr/Ba values may suggest increased depths and higher salinity levels in saltwater environments (Qureshi et al., 2023). Sr/Ba ratios exceeding 0.5 suggest that deposition occurs in a marine environment, while ratios between 0.2 and 0.5 indicate deposition in brackish water (Wei and Algeo, 2020; Omietimi et al., 2022). Values below 0.2 are indicative of terrestrial deposition. A low 100*Mg/Al ratio (less than 1.0) suggests that the deposition occurred in a freshwater paleosedimentary environment, free from seawater influence. Ratios ranging from 1 to 10 imply a brackish environment, while values exceeding 10.0 indicate marine conditions. Additionally, elevated Ca/Al ratios may signify marine or evaporite influences, whereas lower ratios are suggestive of terrestrial (freshwater) conditions.

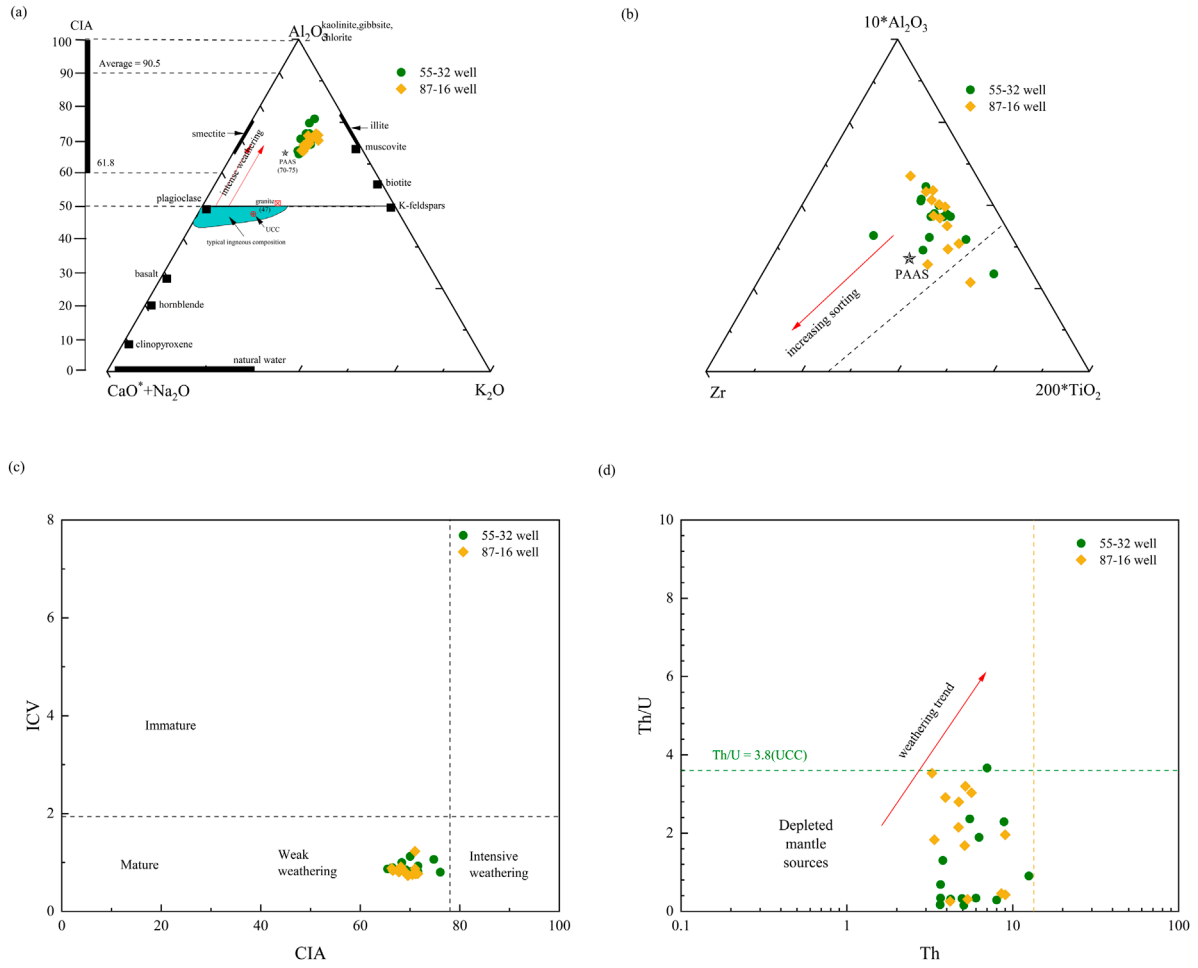

FIGURE 11
Diagrams showing the paleoweathering intensity on the source rocks of the studied sandstones. These diagrams are **(a)** Al_2O_3–(CaO^* + Na_2O)–K_2O ternary diagram of Nesbitt and Young (1982). Red arrow indicates predicted ideal weathering trend (Nesbitt and Young, 1984). The red arrow indicates diagenetic K-metasomatism trend (Fedo et al., 1995). The average composition of UCC and PAAS are from Taylor and McLennan (1985), **(b)** Al_2O_3–Zr–TiO_2 ternary diagram (after Garcia et al., 1991), **(c)** ICV versus CIA bivariate diagram (after McLennan et al., 1993) and **(d)** Th versus Th/U bivariate diagram (after McLennan et al., 1993).

Paleosalinity significantly affects organism growth and the accumulation and preservation of organic material. This relationship is particularly crucial for the paleoproductivity of both cores. In the Zhiluo Formation 55-32 core, the Sr/Ba ratios range from 0.28 to 0.39, averaging 0.32, which suggests a brackish depositional environment. Similarly, the 87-16 core, also indicative of a brackish environment, exhibits Sr/Ba levels between 0.27 and 0.33, with an average of 0.29 (Figure 12a).

The 100*Mg/Al values in the 55-32 core range from 8.71 to 16.5, with an average of 12.25, while the Ca/Al concentrations vary between 0.05 and 0.14, averaging 0.08. These findings indicate that the deposition of the Zhiluo Formation occurred in a brackish to marine environment. Similarly, the 87-16 core exhibits comparable 100*Mg/Al concentrations, ranging from 8.81 to 17.82, with an average of 11.19, and Ca/Al ratios from 0.05 to 0.16, averaging 0.08. This also suggests the presence of brackish to marine conditions (Figure 12b). Climate factors, including chemical alterations and paleosalinity, significantly influence environmental conditions in sedimentary environments (Yan et al., 2021; Yang et al., 2023). A cross-plot analysis was conducted to explore the relationship between climate indicators and salinity proxies. This analysis reveals how climate variations impact salinity levels (Figure 12c). Our research revealed a decrease in salinity levels during predominantly arid conditions (Figure 12c).

5.4.2 Palaeoredox conditions

Geochemical proxies for trace elements such as U/Th, Ni/Co., and V/Cr have demonstrated their effectiveness in assessing the paleoredox conditions of sedimentary rocks. These proxies offer valuable insights into the nature of sediment deposition, indicating whether it took place under oxic or anoxic conditions (Bai et al., 2015; Xie et al., 2018; Liang et al., 2020; Yan et al., 2021; Qureshi et al., 2023). The U/Th ratio was utilized to assess the redox conditions of the Zhiluo Formation based on subsurface data obtained from both cores. A ratio exceeding 1.25 signifies an anoxic environment, whereas a ratio ranging from 0.75 to 1.25 indicates a transition

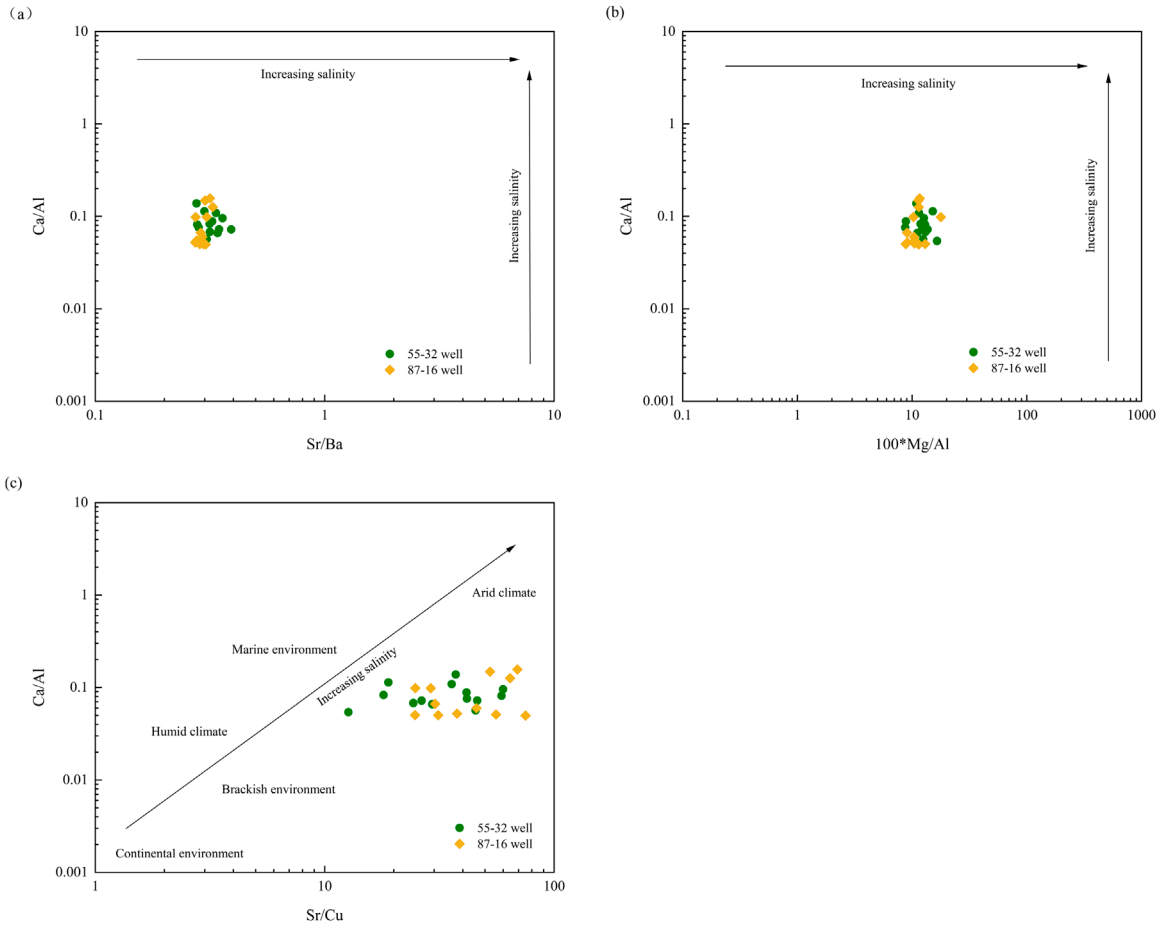

FIGURE 12
Diagrams showing the salinity conditions within the study area. **(a)** Plot of Sr/Ba vs Ca/Al showing the paleosalinity of the Araromi Formation; **(b)** crossplot of 100*Mg/Al vs Ca/Al indicating salinity conditions; **(c)** Sr/Cu vs Ca/Al plot showing the relationship between climate and salinity levels.

from suboxic to dysoxic conditions (Bai et al., 2015; Liang et al., 2020). Conversely, a ratio below 0.75 signifies an oxic environment (Bai et al., 2015). Oxic conditions are indicated by a Ni/Co. ratio of less than 5, while sub-oxic to anoxic environments are typically observed when the ratio exceeds 5 (Qureshi et al., 2023). The V/Cr ratio serves as an important indicator of environmental conditions. A ratio exceeding 4.0 indicates an anoxic environment, while a ratio ranging from 2.0 to 4.0 suggests a transition from suboxic to dysoxic conditions. Conversely, values falling below 2.0 are indicative of an oxic environment.

The average U/Th ratios of 2.34 and 1.19 for the 55–32 and 87–16 cores, respectively, indicate low paleo-oxygenation levels, suggesting that deposition primarily occurred in an anoxic to suboxic environment. A few samples from the 87-16 core exhibited oxic conditions. Similarly, the mean Ni/Co. and V/Cr ratios were lower than the UCC concentrations, further indicating reduced oxygen levels during deposition.

The index yield provides insights into the prevailing redox conditions during sediment deposition. The ash yield index varies from 0.05 to 0.14, indicating weak reducing conditions, whereas a range of 0.23–1.23 suggests a more significantly reducing aquatic environment (He et al., 2022). In the sandstone of the Zhiluo Formation, the ash yield index values exhibit a range from 0.11 to 1.37, with an average of 0.08 for the 55-32 core. This data indicates a weak reducing water environment prevailing during both deposition and diagenesis. Similarly, the samples from the 87-16 core demonstrate ash yield index values between 0.04 and 0.14, with a mean of 0.06, further suggesting comparable weak reducing conditions during the deposition phase.

5.4.3 Paleoweathering and paleoclimatology

Chemical weathering of clastic rocks serves as a valuable method for monitoring paleoclimatic variations throughout the process of sediment deposition (Nesbitt and Young, 1982; Chukwuma et al., 2022; Omietimi et al., 2022; Tang et al., 2023; Qureshi et al., 2023). The indicators demonstrate the overall variations in weathering intensity within the source region, which frequently shifts between arid-cold and humid-warm climatic conditions (Perri and Ohta, 2014; Krzeszowska, 2019; Bokanda et al., 2021; Tang et al., 2023; Zhang et al., 2023). The CIA serves as a dependable proxy indicator for climatic conditions, as it quantifies the ratio of alumina to labile oxides, which directly reflects the degree of chemical weathering (Chukwuma et al., 2022). Intense chemical weathering, characterized by CIA values ranging from 85 to 100, is typically

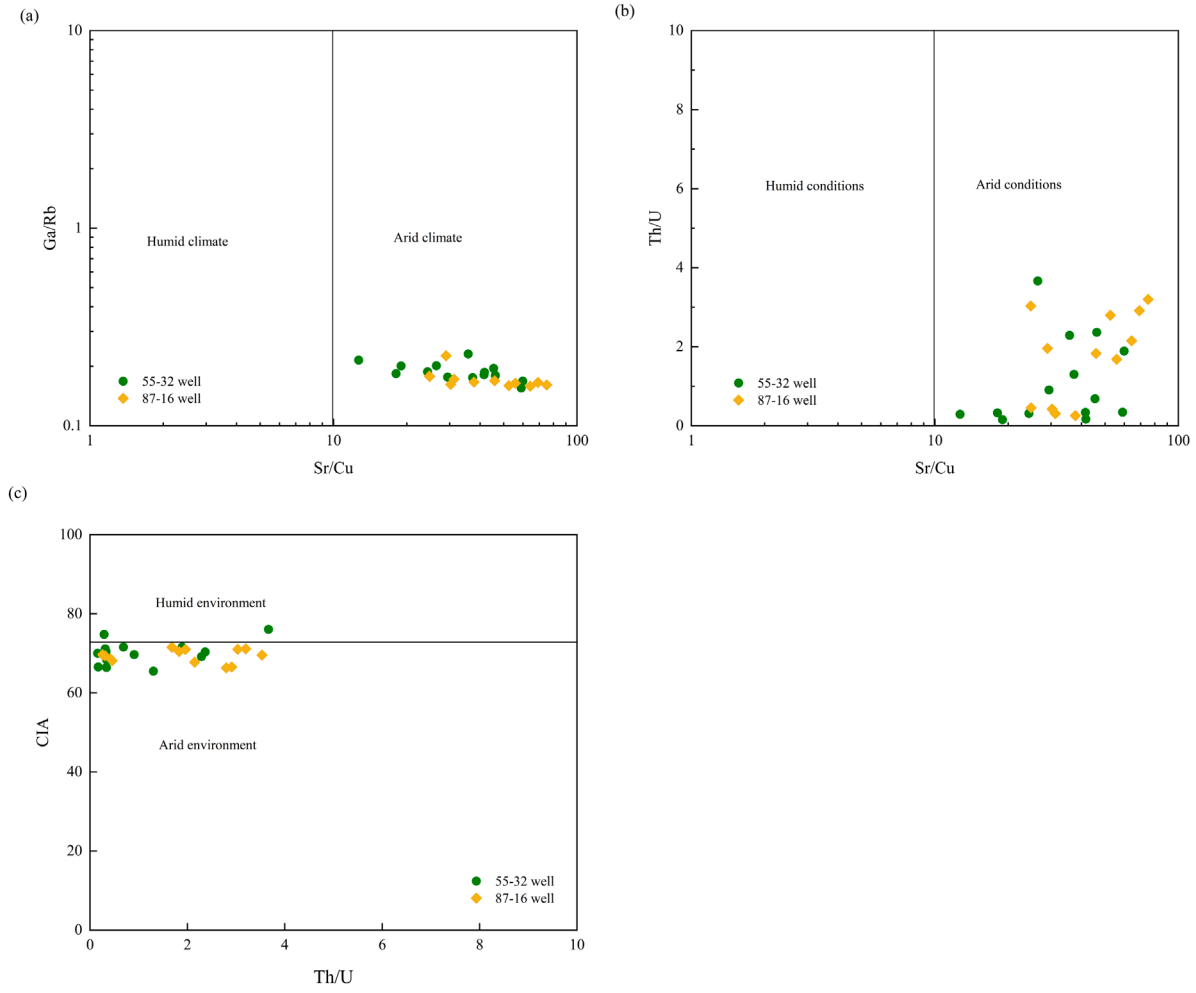

FIGURE 13
Climate interpretation of the Zhiluo Formation from elemant data. **(a)** Sr/Cu vs Ga/Rb; **(b)** Sr/Cu vs Th/U; **(c)** Thu/U vs CIA.

associated with hot and humid climates that promote significant rainfall (Omietimi et al., 2022). A CIA value between 65 and 85 indicates a warm, humid environment typical of moderate chemical weathering. In contrast, a CIA value below 65 suggests low chemical weathering, which is commonly linked to arid conditions with reduced precipitation (Hu et al., 2016; Ngueutchoua et al., 2019).

The analysis of the samples from the 55-32 core indicates a moderate degree of chemical weathering, with Chemical Index of Alteration (CIA) values ranging from 65.49 to 76.08, and an average of 70.12. Similarly, the samples from the 87-16 core exhibit a comparable moderate degree of chemical weathering, with CIA values fluctuating between 66.32 and 71.56, averaging 69.32. These CIA values imply a period characterized by warm and humid climatic conditions during the sedimentation of the Middle Jurassic Zhiluo Formation. To illustrate the impact of climatic variation on the weathering processes and geochemical maturity of clastic rocks, a cross-graph depicting the Index of Compositional Variability (ICV) against the Chemical Index of Alteration (CIA) was employed (Figure 11c). The data suggest a direct correlation between climate and geochemical maturity, as well as paleoweathering processes. A humid climate is associated with the development of mature clastic rocks and heightened chemical weathering. Conversely, sedimentary rocks characterized by low chemical weathering and geochemical immaturity are typically found in arid and elevated temperature environments (Figure 11c).

To gain a thorough understanding of the Middle Jurassic paleoclimate along the northern margin of the Ordos Basin, it is essential to go beyond conventional parameters and incorporate a variety of geochemical indicators. In addition to traditional data sources, several supplementary geochemical markers of climate change were utilized to enhance our comprehension of the region's paleoclimate. Previous studies have demonstrated that analyzing the relative concentrations and distributions of trace elements in mudrocks can effectively reconstruct the paleoclimatic conditions present during their deposition.

In sedimentary research, the ratios of Ga/Rb, Th/U, Sr/Cu, Rb/Sr, and SiO2/Al2O3 in fine-grained sedimentary rocks are widely recognized as dependable indicators for assessing paleoclimatic conditions (Xie et al., 2018; Baioumy et al., 2021; Hussain et al., 2021; Al-Juboury et al., 2021; Omietimi et al., 2022; Fathy et al., 2023). Trace elements such as gallium (Ga), rubidium (Rb),

TABLE 4 (*Continued*) Rare earth element concentrations (ppm) and ratios of analysed samples.

Sample no.	La	Ce	Pr	Nd	Sm	Eu	Gd	Tb	Dy	Ho	Er	Tm	Yb	Lu	Y	∑REEs	∑LREEs	∑HREEs	∑LREEs/∑HREEs	Eu/Eu*	Ce/Ce*	La/Yb	(La/Yb)cn	(La/Sm)cn	(Gd/Yb)cn
S23	27.20	50.00	5.84	21.50	3.38	1.12	2.84	0.42	1.89	0.31	1.00	0.15	0.93	0.13	7.48	124.19	109.04	15.15	7.20	1.01	0.90	29.34	16.71	5.07	2.47
S24	37.70	68.00	7.93	28.50	4.40	1.08	3.53	0.55	2.54	0.43	1.40	0.23	1.51	0.21	10.9	168.90	147.61	21.29	6.93	0.76	0.88	24.97	14.22	5.39	1.89
S25	40.40	74.80	8.43	31.10	4.84	1.17	3.99	0.59	2.72	0.46	1.46	0.23	1.44	0.20	11.6	183.43	160.74	22.69	7.08	0.74	0.91	28.06	15.98	5.25	2.24
S26	26.70	47.10	5.57	20.80	3.42	0.98	2.77	0.40	1.84	0.30	0.95	0.13	0.84	0.12	7.82	119.74	104.57	15.17	6.89	0.89	0.87	31.64	18.02	4.91	2.65
S27	23.80	43.30	5.19	18.90	3.05	1.05	2.57	0.38	1.68	0.29	0.88	0.13	0.81	0.12	7.27	109.42	95.29	14.13	6.75	1.04	0.88	29.31	16.69	4.91	2.55
Average	30.29	53.74	6.14	22.51	3.55	1.17	2.98	0.45	2.16	0.39	1.17	0.19	1.20	0.17	10.11	136.21	117.40	18.81	6.32	1.04	0.87	26.10	14.86	5.39	2.06
UCC[a]	31.00	63.00	7.10	27.00	4.70	1.00	4.00	0.70	3.90	0.83	2.30	0.30	2.00	0.31	21	169.14	133.80	35.34	3.79	0.64	0.97	15.50	8.83	4.15	1.61
PAAS[b]	38.20	80.00	8.90	32.00	5.60	1.10	4.70	0.77	4.40	1.00	2.90	0.40	2.80	0.43	—	—	165.80	—	—	0.60	0.99	13.64	7.77	4.29	1.35

UCC[a]: average Upper Continental Crust (Rudnick and Gao, 2003).
PAAS[b]: average post-Archean Australian Shale (McLennan, 1989).

strontium (Sr), and thorium (Th), along with major oxides like manganese (Mn), aluminum (Al), magnesium (Mg), and calcium (Ca), exhibit sensitivity to variations in paleoclimatic conditions (Moradi et al., 2016; Xie et al., 2018; Omietimi et al., 2022). Gallium (Ga) is primarily linked to the fine-grained aluminosilicate fraction and is found in higher concentrations within clastic rocks associated with kaolinite. This suggests the presence of warm and humid climatic conditions (Xie et al., 2018; Hussain et al., 2021). Rubidium (Rb) is often linked to illite, suggesting a reduced level of chemical weathering that aligns with arid and cold climatic conditions (Xie et al., 2018). The Ga/Rb ratio in clastic rocks generally declines as conditions transition to colder and drier climates (Fathy et al., 2023).

The ratios of Sr/Cu and Ga/Rb exhibit significant positive correlations in siliciclastic rocks. In warm and humid climates, these deposits tend to display elevated Ga/Rb ratios alongside reduced Sr/Cu ratios (Xie et al., 2018). The Sr/Cu ratio serves as a dependable indicator of paleoclimatic conditions. Elevated Sr/Cu ratios typically imply an arid climate, while ratios below 5.0 suggest a warm and humid environment. Ratios ranging from 5.0 to 10.0 indicate semi-arid to semi-humid conditions, whereas values exceeding 10.0 point to an arid climate (Xie et al., 2018; Omietimi et al., 2022). Moreover, strong chemical weathering, which is mostly caused by uranium (U) oxidation, raises the Th/U ratios (McLennan et al., 1993). U^{4+} easily oxidized to U^{6+} during weathering during Th and U fractionation. The Th/U ratios rise as a result of the repeated cycles of weathering and re-deposition, making them useful markers of these intricate geological processes (Taylor and McLennan, 1985). Low chemical weathering in arid conditions is indicated by a Th/U ratio less than 3. On the other hand, high Th/U values signify a warm, humid climate (Moradi et al., 2016; Shen et al., 2015). Climate differences have an impact on the Rb/Sr ratio; high ratios imply dry, cold circumstances, whereas low ratios indicate warm conditions (Bai et al., 2015). Furthermore, SiO_2/Al_2O_3 ratios have been successful in describing chemical changes and paleoclimate conditions (Xu et al., 2022). Moreover, owing to the responsive nature of major oxide contents (such as SiO_2, Al_2O_3, K_2O, and Na_2O) to climate changes, low SiO_2/Al_2O_3 ratios serve as indicators of warm and humid climates (Moradi et al., 2016; Xu et al., 2022). In this study, climate indicators such as Ga/Rb, Th/U, Sr/Cu, Rb/Sr and SiO_2/Al_2O_3 ratios, were utilised to reconstruct the paleoclimate evolution during the Middle Jurassic in the Ordos Basin.

Figure 13 a illustrates that the Ga/Rb amounts for the Middle Jurassic Zhiluo Formation samples from the 55-32 core range from 0.16 to 0.23 (average 0.19), while those for the 87-16 core samples range from 0.15 to 0.23 (average 0.17). The 87-16 core has a Sr/Cu ratio of 24.75–112.18 (average 49.58) and the 55-32 core has a ratio of 12.69–59.87 (average 35.47). The samples' Ga/Rb and Sr/Cu ratios point to an arid environment in the Ordos Basin when the Middle Jurassic Zhiluo Formation was being deposited. Furthermore, the cross-plot of Sr/Cu vs Th/U ratios also supports arid climatic conditions (Figure 13b). Also, the cross-plot of CIA vs Th/U ratios provides further evidence that supports the arid climate (Figure 13c).

5.5 Sedimentary recycling

The Zhiluo Formation's high concentration of feldspar and rock pieces, low roundness, and poor sorting all point to the sandstones' immaturity. The recycling and maturity of sediments are assessed using the index of compositional variability (ICV). The ICV index is calculated as follows (the oxides are calculated by percentages): ICV = (TFe_2O_3 + K_2O+ Na_2O+ CaO + TiO_2)/Al_2O_3 (Cox et al., 1995).

A low ICV value corresponds to a high clay mineral content (Cox et al., 1995). The ICV value is greater than 1 for the first-cycle products in the tectonically active region. With ICV values less than 0.84, the rocks rich in alteration minerals (kaolinite, muscovite, and illite) underwent severe weathering and several sedimentary cycles and were typically deposited in tectonically calm areas (Cox et al., 1995). The PAAS (0.80) is much lower than the ICV of the Zhiluo Formation in the 55-32 and 87-16 wells, which range from 0.80 to 1.12 (mean, 0.89) and 0.73 to 1.23 (mean, 0.84). The Zhiluo Formation is first-cycle and compositionally immature, according to these values.

Th and Sc are chemically stable during deposition, and no fractionation occurs (Mclennan and Taylor, 1991). The Zr/Sc ratio can reveal recycled sediments, while the Th/Sc ratio shows the compositional diversity of igneous rocks (Taylor and McLennan, 1985). The diagram of Th/Sc versus Zr/Sc can reflect the sedimentary cycle effectively (McLennan et al., 1993; Asiedu et al., 2000). As zircon is enriched during the transit and sedimentation processes, the Zr/Sc ratio progressively rises (Asiedu et al., 2000). Therefore, the degree of zircon enrichment can be ascertained by the Zr/Sc ratio. Parallel to Trend 1, the Zr/Sc ratio of the sandstones of the Zhiluo Formation has a positive correlation with Th/Sc (Figure 6d). This demonstrated that there was no Zr enrichment and that the sandstones were immature since their Zr concentration was lower than that of the higher crust. As a result, the sandstones of the Zhiluo Formation might be first-cycle and have come from a volcanic source region where tectonics is active.

6 Uranium mineralization

The overall structural environment during the sedimentation period of the Zhiluo Formation was stable. The overall structure is loose sandstone, mainly composed of medium to fine-grained sandstone, with low compositional maturity, poor cementation, good porosity and connectivity, and large-scale lateral connectivity. The top and bottom mudstone aquitards are stable. These features are beneficial for the transportation of uranium and oxygen containing water and the formation of uranium ore bodies. In addition, due to the abundant uranium supply in the parent rock and erosion source area, a certain degree of uranium pre enrichment occurred during the sedimentation of the Zhiluo Formation sand body. Clay minerals and organic sedimentary debris in sandstone adsorb and fix a large amount of uranium before enrichment or early mineralization. In complex geological historical processes such as sedimentation, uranium containing fluids undergo complex adsorption reduction deposition processes with changes in physical and chemical conditions. According to previous research, firstly, the Zhiluo Formation sandstone will undergo a weak reducing water environment, during which the reducing conditions are weak, tectonic activity is not developed, and the overall climate conditions are arid, but it will experience a warm and humid climate period. During the transition of arid, semi-arid, and warm humid climates in ancient times, the strata were rich in organic carbon. When the uranyl complex ions in the geological fluids rich in the strata released uranium near certain geochemical barriers, they were adsorbed by good adsorbents such as pyrite, organic matter, and other clay minerals. In a slightly salty reducing environment, U^{6+}combined with $Si^{4+}$and $Ti^{4+}$to form coffinite and uranium titanium oxide.

7 Conclusion

This study demonstrates how the lithofacies and geochemical characteristics of sandstone can successfully identify its evidence, as well as how to decipher the tectonic background, paleoclimate, and paleoweathering of its source area (rock). The integration of mineral lineages and geochemical data of the studied sandstone indicates that the detrital particles of sandstone mainly come from multiple recycled felsic (granite) igneous source rocks, followed by intermediate igneous rocks (granodiorite), metamorphic rocks (gneiss), and mafic igneous rocks (andesite). Based on the resulting lithofacies, block rock geochemistry, and characteristic ratios of La/Sc, Th/Sc, and Co./Th, the Bayinqinggeli sandstone is derived from felsic lithology (granite and gneiss) and regenerated quartz sediment sources. The standardized REE distribution pattern of chondrite meteorites in Bayinqinggelli sandstone shows enriched LREE and flat HREE, with negative Eu/Eu*anomalies, similar to UCC characterized by felsic rocks. In terms of paleoweathering and paleoclimate in the source area, geochemical indicators and ratios of trace elements such as Th/U and Th/Sc indicate that the source area has undergone moderate to severe chemical weathering, mainly occurring under arid climatic conditions, but also experiencing warm, semi humid to humid climatic conditions.

Data availability statement

The original contributions presented in the study are included in the article/supplementary material, further inquiries can be directed to the corresponding author.

Author contributions

XL: Writing – original draft, Writing – review and editing. SP: Writing – review and editing, Investigation. ZL: Resources, Writing – review and editing. FH: Project administration, Writing – review and editing. XL: Methodology, Writing – review and editing. ZZ: Resources, Writing – review and editing.

Funding

The author(s) declare that financial support was received for the research and/or publication of this article. This study was funded

by the CNNC Young Excellence Programme (NO. QNYC2301) and the National Nature Science Foundation of China (Grant number U2167210). The authors declare that this study received funding from CNNC. The funder was not involved in the study design, collection, analysis, interpretation of data, the writing of this article, or the decision to submit it for publication.

Acknowledgments

The editors and reviewers are gratefully acknowledged.

Conflict of interest

Authors XL, ZL, FH, XL, and ZZ were employed by China National Nuclear Corporation (CNNC).

The remaining author declares that the research was conducted in the absence of any commercial or financial relationships that could be construed as a potential conflict of interest.

Generative AI statement

The author(s) declare that no Generative AI was used in the creation of this manuscript.

Publisher's note

All claims expressed in this article are solely those of the authors and do not necessarily represent those of their affiliated organizations, or those of the publisher, the editors and the reviewers. Any product that may be evaluated in this article, or claim that may be made by its manufacturer, is not guaranteed or endorsed by the publisher.

References

Al-Juboury, A. I., Hussain, S. H., and Al-Lhaebi, S. H. (2021). Geochemistry and mineralogy of the Silurian Akkas Formation, Iraqi western desert: implications for palaeoweathering, provenance and tectonic setting. *Arab. J. Geosci.* 14, 760. doi:10.1007/s12517-021-06887-w

Alqahtani, F. A., and Khalil, M. (2019). Geochemical analysis and tectonic evaluation of the miocene–pliocene sequence at Al rehaili area, northern jeddah, Saudi arabia. *Arabian J. Geosciences* 12, 323. doi:10.1007/s12517-019-4491-0

Alqahtani, F. A., and Khalil, M. (2021). Geochemical analysis for evaluating the paleoweathering, paleoclimate, and depositional environments of the siliciclastic Miocene-Pliocene sequence at Al-Rehaili area, Northern Jeddah, Saudi Arabia. *Arabia Arabian J. Geosciences* 14, 239. doi:10.1007/s12517-021-06538-0

Amedjoe, G. C., Gawu, S. K., Ali, B., Aseidu, D. K., and Nude, P. /.M. (2018). Geochemical compositions of Neoproterozoic to Lower Palaeozoic (?) shales and siltstones in the Volta Basin (Ghana): constraints on provenance and tectonic setting. *Sediment. Geol.* 368, 114–131. doi:10.1016/j.sedgeo.2018.03.004

Armstrong-Altrin, J. S., Lee, Y. I., Kasper Zubillaga, J. J., and Trejo Ramírez, E. (2017). Mineralogy and geochemistry of sands along the Manzanillo and El Carrizal beach areas, southern Mexico: implications for palaeoweathering, provenance and tectonic setting. *Geol. J.* 52, 559–582. doi:10.1002/gj.2792

Armstrong-Altrin, J. S., Nagarajan, R., Balaram, V., and Natalhy-Pineda, O. (2015). Petrography and geochemistry of sands from the Chachalacas and Veracruz beach areas, western Gulf of Mexico, Mexico: constraints on provenance and tectonic setting. *J. S. Am. Earth Sciences* 64, 199–216. doi:10.1016/j.jsames.2015.10.012

Asiedu, D. K., Suzui, S., and Shibata, T. (2000). Provenance of sandstones from the lower cretaceous sasayama group, inner zone of southwest Japan. *Sediment. Geol.* 131, 9–24. doi:10.1016/s0037-0738(99)00122-0

Augustsson, C., Aehnelt, M., Olivarius, M., Voigt, T., Gaupp, H., and Hilse, U. (2023). Provenance from the geochemical composition of terrestrial clastic deposits — a review with case study from the intracontinental Permo-Triassic of European Pangea. *Sediment. Geol.* 456, 106496. doi:10.1016/j.sedgeo.2023.106496

Bai, Y., Liu, Z., Sun, P., Liu, R., Hu, X., Zhao, H., et al. (2015). Rare earth and major element geochemistry of Eocene fine-grained sediments in oil shale-and coal-bearing layers of the Meihe Basin, Northeast China. *J. Asian Earth Sci.* 97, 89–101. doi:10.1016/j.jseaes.2014.10.008

Baioumy, H., Salim, A. M. A., Ahmed, N., Maisie, M., and Al-Kahtany, K. (2021). Upper cretaceous-upper Eocene mud-dominated turbidites of the belaga formation, sarawak (Malaysia): 30Ma of paleogeographic, paleoclimate and tectonic stability in sundaland. *Mar. Petrol. Geol.* 126, 104897. doi:10.1109/ICRA48506.2021.956200

Basu, A., Young, S., Suttner, L., James, W., and Mack, G. (1975). Re-evaluation of the use of undulatory extinction and crystallinity in detrital quartz for provenance interpretation. *J. Sediment. Res.* 45, 873–882. doi:10.1306/212F6E6F-2B24-11D7-8648000102C1865D

Bhatia, M. R. (1983). Plate tectonics and geochemical composition of sandstones. *J. Geol.* 91, 611–627. doi:10.1086/628815

Bhatia, M. R., and Crook, K. W. (1986). Trace element characteristics of graywackes and tectonic setting discrimination of sedimentary basins. *Contributions Mineralogy Petrology* 92, 181–193. doi:10.1007/bf00375292

Bokanda, E. E., Fralick, P., Ekomane, E., Bisse, S. B., Tata, C. N., Ashukem, E. N., et al. (2021). Geochemical constraints on the provenance, paleoweathering and maturity of the Mamfe black shales, West Africa. *J. Afr. Earth Sci.* 175, 104078. doi:10.1016/j.jafrearsci.2020.104078

Bracciali, L., Marroni, M., Pandolfi, L., and Rocchi, S. (2007). "Geochemistry and petrography of Western Tethys Cretaceous sedimentary covers (Corsica and Northern Apennines): from source areas to configuration of margins,". *Sedimentary Provenance and Petrogenesis: Perspectives from Petrography and Geochemistry Geological Society of America, Special Paper*. Editors J. Arribas, S. Critelli, and M. J. Johnsson 420, 73–93.

Chen, L., Jiang, S., Chen, P., Chen, X., Zhang, B., Zhang, G., et al. (2021). Relative sea-Level changes and organic matter enrichment in the upper ordovician- lower silurian wufeng-longmaxi formations in the central yangtze area, China. *Mar. Pet. Geol.* 124, 104809. doi:10.1016/j.marpetgeo.2020.104809

Chukwuma, K., Tsikos, H., Wagner, N., and Frazenburg, M. (2022). Dual sea-level-climatic controls on the stratigraphic distribution of total organic carbon content and macerals in the Permian black shales of southwest Gondwana. *J. Afr. Earth Sci.* 188, 104495. doi:10.1016/j.jafrearsci.2022.104495

Cox, R., Lowe, D. R., and Cullers, R. L. (1995). The influence of sediment recycling and basement composition on evolution of mudrock chemistry in the south-western United States. *Geochimica Cosmochimica Acta* 59, 2919–2940. doi:10.1016/0016-7037(95)00185-9

Critelli, S., Arribas, J., Le Pera, E., Tortosa, A., Marsaglia, K. M., and Latter, K. K. (2003). The recycled orogenic sand provenance from an uplifted thrust belt, Betic Cordillera, southern Spain. *J. Sediment. Res.* 73, 72–81. doi:10.1306/071002730072

Cullers, R. L. (1994). The controls on the major and trace element variation of shales, siltstones, and sandstones of Pennsylvanian–Permian age from uplifted continental blocks in Colorado to platform sediment in Kansas, USA. *Geochimica Cosmochimica Acta* 58, 4955–4972. doi:10.1016/0016-7037(94)90224-0

Cullers, R. L. (2000). The geochemistry of shales, siltstones and sandstones of Pennsylvanian–Permian age, Colorado, USA: implications for provenance and metamorphic studies. *Lithos* 51, 181–203. doi:10.1016/s0024-4937(99)00063-8

Dickinson, W. R. (1970). Interpreting detrital modes of graywacke and arkose. *J. Sediment. Petrology* 40, 695–707. doi:10.1306/74D72018-2B21-11D7-8648000102C1865D

Dickinson, W. R., Beard, L. S., Brakenridge, G. R., Erjavec, J. L., Ferguson, R. C., Inman, K. F., et al. (1983). Provenance of North American Phaner ozoic sandstones in relation to tectonic setting. *Geol. Soc. Am. Bull.* 94, 222–235. doi:10.1130/0016-7606(1983)94<222:ponaps>2.0.co;2

Dickinson, W. R., and Suczek, C. A. (1979). Plate tectonics and sandstone compositions. *Am. Assoc. Petroleum Geol. Bullen* 63, 2164–2182. doi:10.1306/2f9188fb-16ce-11d7-8645000102c1865d

Fathy, D., Abart, R., Wagreich, M., Gier, S., Ahmed, M. S., and Sami, M. (2023). Late campanian climatic-continental weathering assessment and its influence on source rocks deposition in southern Tethys, Egypt. *Minerals* 13, 160. doi:10.3390/min13020160

Fathy, D., Wagreich, M., Ntaflos, T., and Sami, M. (2021). Paleoclimatic variability in the southern Tethys, Egypt: insights from the mineralogy and geochemistry of Upper Cretaceous lacustrine organic-rich deposits. *Cretac. Res.* 126, 104880. doi:10.1016/j.cretres.2021.104880

Fedo, C. M., Nesbitt, H. W., and Young, G. M. (1995). Unravelling the effects of potassium metasomatism in sedimentary rocks and paleosols, with implications for aleoweathering conditions and provenance. *Geology* 23, 921–924. doi:10.1130/0091-7613(1995)023<0921:UTEOPM>2.3.CO;2

Floyd, P. A., and Leveridge, B. E. (1987). Tectonic environment of the Devonian Gramscatho basin, south Cornwall: framework mode and geochemical evidence from turbiditic sandstones. *J. Geol. Soc. Lond.* 144, 531–542. doi:10.1144/gsjgs.144.4.0531

Gaillardet, J., Dupré, B., and Allègre, C. (1999). Geochemistry of large river suspended sediments: silicate weathering or recycling tracer? *Geochimica Cosmochimica Acta* 63, 4037–4051. doi:10.1016/s0016-7037(99)00307-5

Garcia, D., Coelho, J., and Perrin, M. (1991). Fractionation between TiO2 and Zr as a measure of sorting within shale and sandstone series (northern Portugal). *Eur. J. Mineralogy* 3, 401–414. doi:10.1127/ejm/3/2/0401

Harnois, L. (1988). The CIW index: a new chemical index of weathering. *Sediment. Geol.* 55, 319–322. doi:10.1016/0037-0738(88)90137-6

Hayashi, K., Fujisawa, H., Holland, H., and Ohmoto, H. (1997). Geochemistry of ~1.9 Ga sedimentary rocks from northeastern Labrador, Canada. *Geochimica Cosmochimica Acta* 61, 4115–4137. doi:10.1016/s0016-7037(97)00214-7

He, W., Tao, S., Hai, L., Tao, R., Wei, X., and Wang, L. (2022). Geochemistry of the tanshan oil shale in jurassic coal measures, western ordos basin: implications for sedimentary environment and organic matter accumulation. *Energies* 15, 8535. doi:10.3390/en15228535

Herron, M. M. (1988). Geochemical classification of terrigenous sands and shales from core or log data. *J. Sediment. Res.* 58, 820–829. doi:10.1306/212F8E77-2B24-11D7-8648000102C1865D

Hiscott, R. (1984). Ophiolitic source rocks for Taconic-Age flysch: trace-element evidence. *Geol. Soc. Am. Bull.* 95, 1261–1267. doi:10.1130/0016-7606(1984)95<1261:osrftf>2.0.co;2

Hu, J., Li, Q., Li, J., Huang, J., and Ge, D. (2016). Geochemical characteristics and depositional environment of the Middle Permian mudstones from central Qiangtang Basin, northern Tibet. *Geol. J.* 51, 560–571. doi:10.1002/gj.2653

Hussain, S. H., Al-Juboury, A. I., Al-Haj, M. A., Armstrong-Altrin, J. S., and Al-Lhaebi, S. F. (2021). Mineralogy and geochemistry of the late triassic baluti formation, northern Iraq. *J. Afr. Earth Sci.* 181, 104243. doi:10.1016/j.jafrearsci.2021.104243

Ivanova, V. V., Nikol'skii, P. A., Tesakov, A. S., Basilyan, A. E., Belolyubskii, I. N., and Boeskorov, G. G. (2015). Geochemical indicators of paleoclimatic changes in the cenozoic deposits of the lower aldan basin. *Geochem. Int.* 53, 358–368. doi:10.1134/s0016702915020044

Kroonenberg, S. B. (1994). "Effects of provenance, sorting and weathering on the geochemistry of fluvial sands from different tectonic and climatic environments," in *Proceedings of the 29th international geological congress, Part A*, 69–81.

Krzeszowska, E. (2019). Geochemistry of the lublin Formation from the lublin coal basin: implications for weathering intensity, palaeoclimate and provenance. *Int. J. Coal Geol.* 216, 103306. doi:10.1016/j.coal.2019.103306

Le Bas, M. J., Le Maitre, R. W., Streckeisen, A., and Zanettinal, B. (1986). A chemical classification of volcanic rocks based on the total alkali–silica diagram. *J. Petrology* 27, 745–750. doi:10.1093/petrology/27.3.745

Liang, Q., Tian, J., Zhang, X., Sun, X., and Yang, C. (2020). Elemental geochemical characteristics of lower—middle permian mudstones in taikang uplift, southern north China basin: implications for the FOUR-PALEO conditions. *Geosci. J.* 24, 17–33. doi:10.1007/s12303-019-0008-9

Long, X., Yuan, C., Sun, M., Xiao, W., Wang, Y., Cai, K., et al. (2012). Geochemistry and Nd isotopic composition of the Early Paleozoic flysch sequence in the Chinese Altai, Central Asia: evidence for a northward-derived mafic source and insight into Nd model ages in accretionary orogen. *Gondwana Res.* 22, 554–566. doi:10.1016/j.gr.2011.04.009

Löwen, K., Meinhold, G., and Güngör, T. (2018). Provenance and tectonic setting of Carboniferous–Triassic sandstones from the Karaburun Peninsula, western Turkey: a multimethod approach with implications for the Palaeo-Tethys evolution. *Sediment. Geol.* 375, 232–255. doi:10.1016/j.sedgeo.2017.11.006

Ma, S., Li, J., Wang, L., Gao, H., and Zhang, J. (2021). Provenance, tectonic setting and source-area paleoweathering of the Upper Paleozoic sandstones in the northwestern Ordos Basin, China: evidence from whole-rock geochemistry. *Carbonates Evaporites* 36, 64. doi:10.1007/s13146-021-00729-2

McLennan, S. M. (1989). Rare earth elements in sedimentary rocks: influence of provenance and sedimentary processes. *Rev. Mineralogy Geochem.* 21, 169–200. doi:10.1515/9781501509032-010

McLennan, S. M. (2001). Relationships between the trace element composition of sedimentary rocks and upper continental crust. *Geochem. Geophys. Geosystems* 2, 1021. doi:10.1029/2000gc000109

McLennan, S. M., Hemming, S., McDaniel, D. K., and Hanson, G. N. (1993). "Geochemical approaches to sedimentation, provenance, and tectonics,". *Processes controlling the composition of clastic sediments*. Editors M. J. Johnsson, and A. Basu (Boulder, Colorado: Geological Society of America, Special Paper), 284, 21–40. doi:10.1130/spe284-p21

McLennan, S. M., and Taylor, S. R. (1980). Th and U in sedimentary rocks: crustal evolution and sedimentary recycling. *Nature* 285, 621–624. doi:10.1038/285621a0

McLennan, S. M., and Taylor, S. R. (1991). Sedimentary rocks and crustal evolution: tectonic setting and secular trends. *J. Geol.* 99, 1–21. doi:10.1086/629470

Moghaddam, S. P., Salehi, M. A., Jafarzadeh, M., and Zohdi, A. (2020). Provenance, palaeoweathering and tectonic setting of the Ediacaran Bayandor Formation in NW Iran: implications for the northern Gondwana continental margin during the late Neoproterozoic. *J. Afr. Earth Sci.* 161, 103670. doi:10.1016/j.jafrearsci.2019.103670

Moradi, A. V., Sarı, A., and Akkaya, P. (2016). Geochemistry of the Miocene oil shale (Hançili Formation) in the Çankırı-Çorum Basin, Central Turkey: implications for Paleoclimate conditions, source–area weathering, provenance and tectonic setting. *Sediment. Geol.* 341, 289–303. doi:10.1016/j.sedgeo.2016.05.002

Nechaev, V. P., and Isohording, W. C. (1993). Heavy mineral assemblages of continental marginsb as indicators of plate tectonics environment. *J. Sediment. Petrology* 63, 1110–1117. doi:10.1306/D4267CB7-2B26-11D7-8648000102C1865D

Nesbitt, H. W., and Young, G. M. (1982). Early Proterozoic climates and plate motions inferred from major element chemistry of lutites. *Nature* 299, 715–717. doi:10.1038/299715a0

Nesbitt, H. W., and Young, G. M. (1984). Prediction of some weathering trends of plutonic and volcanic rocks based on thermodynamic and kinetic considerations. *Geochim. Cosmochim. Acta* 48, 1523–1534. doi:10.1016/0016-7037(84)90408-3

Ngueutchoua, G., Ekoa Bessa, A. Z., Eyong, J. T., Demanou, Z. D., Baba, D. H., and Tchami, N. L. (2019). Geochemistry of cretaceous fine-grained siliciclastic rocks from Upper Mundeck and Logbadjeck Formations, Douala sub-basin, SW Cameroon: implications for weathering intensity, provenance, paleoclimate, redox condition, and tectonic setting. *J. Afr. Earth Sci.* 152, 215–236. doi:10.1016/j.jafrearsci.2019.02.021

Omietimi, E. J. (2022). *Sedimentology, palaeoenvironment and structural interpretation of the cretaceous SW anambra basin*. Nigeria: University of Pretoria. PhD Thesis.

Omietimi, E. J., Lenhardt, N., Yang, R., Gotz, A. E., and Bumby, A. J. (2022). Sedimentary geochemistry of Late Cretaceous-Paleocene deposits at the southwestern margin of the Anambra Basin (Nigeria): implications for paleoenvironmental reconstructions. *Palaeogeogr. Palaeoclimatol. Palaeoecol.*, 600, 111059, doi:10.1016/j.palaeo.2022.111059

Perri, F., and Ohta, T. (2014). Paleoclimatic conditions and paleoweathering processes on mesozoic continental redbeds from western-central mediterranean alpine chains. *Palaeogeogr. Palaeoclimatol. Palaeoecol.* 395, 144–157. doi:10.1016/j.palaeo.2013.12.029

Pettijohn, F. J., Potter, P. E., and Siever, R. (1987). *Sand and sandstones*. 2nd edition. New York: Springer-Verlag, 553.

Quasim, M. A., Absar, N., Psingh, B., Singh, P., Ahmed, F., and Ashok, M. (2023). Geochemistry of mesoproterozoic bijaigarh shale, upper vindhyan group, son valley, India: implications for source area weathering, provenance and tectonic setting. *J. Earth Syst. Sci.* 132, 115. doi:10.1007/s12040-023-02131-z

Qureshi, K. A., Rizwan, M., Janjuhah, H. T., Islam, I., Kontakiotis, G., Bilal, A., et al. (2023). An integrated petrographical and geochemical study of the tredian Formation in the salt and trans-indus surghar ranges, north-west Pakistan: implications for palaeoclimate. *Depositional Rec.* 10 (1), 33–50. doi:10.1002/dep2.255

Roser, B. P., and Korsch, R. J. (1986). Determination of tectonic setting of sandstone–mudstone suites using SiO2 content and K2O/Na2O ratio. *J. Geol.* 94, 635–650. doi:10.1086/629071

Roser, B. P., and Korsch, R. J. (1988). Provenance signatures of sandstone-mudstone suites determined using discriminant function analysis of major-element data. *Chem. Geol.* 67, 119–139. doi:10.1016/0009-2541(88)90010-1

Rudnick, R. L., and Gao, S. (2003). "Composition of the continental crust,". *Treatise on geochemistry*. Editors H. D. Holland, and K. K. Turekian (Oxford: Elsevier-Pergamon), 3, 1–64. doi:10.1016/b0-08-043751-6/03016-4

Sallam, E. S., and Wanas, H. A. (2019). Petrography and geochemistry of the Jurassic siliciclastic rocks in the Khashm El-Galala area (NW Gulf of Suez, Egypt): implication for provenance, tectonic setting and source area paleoweathering. *J. Afr. Earth Sci.* 160, 103607. doi:10.1016/j.jafrearsci.2019.103607

Shen, J., Schoepfer, S. D., Feng, Q., Zhou, L., Yu, J., Song, H., et al. (2015). Marine productivity changes during the end-Permian crisis and Early Triassic recovery. *Earth Sci. Rev.* 149, 136–162. doi:10.1016/j.earscirev.2014.11.002

Sprague, R. A., Melvin, J. A., Conradi, F. G., Pearce, T. J., Dix, M. A., Hill, S. D., et al. (2009). Integration of core-based chemostratigraphy and petrography of the Devonian Jauf Sandstones, Uthmaniya area, Ghawar field, eastern Saudi Arabia. *Search and Discovery*, 34, 20065.

Tang, W., Song, Y., He, W., Tang, Y., Guo, X., Pe-Piper, G., et al. (2023). Petrochemical and geochronological data of Permian-Lower Triassic clastic sedimentary rocks in the northwestern Junggar basin, NW China: implications for provenance, tectonism and paleoclimate. *Mar. Petrol. Geol.* 148, 106027. doi:10.1016/j.marpetgeo.2022.106027

Taylor, S. R., and McLennan, S. M. (1985). *The continental crust: its composition and evolution*. Oxford, UK: Blackwell Publishing, 312.

Totten, M. W., Hanan, M. A., and Weaver, B. L. (2000). Beyond whole-rock geochemistry of shales: the importance of assessing mineralogic controls for revealing tectonic discriminants of multiple sediment sources for the Ouachita Mountain flysch deposits. *Geol. Soc. Am. Bull.* 112, 1012–1022. doi:10.1130/0016-7606(2000)112<1012:bwgost>2.0.co;2

Verma, S. P., and Armstrong-Altrin, J. S. (2013). New multi-dimensional diagrams for tectonic discrimination of siliciclastic sediments and their application to Precambrian basins. *Chem. Geol.* 355, 117–133. doi:10.1016/j.chemgeo.2013.07.014

Verma, S. P., and Armstrong-Altrin, J. S. (2016). Geochemical discrimination of siliciclastic sediments from active and passive margin settings. *Sediment. Geol.* 332, 1–12. doi:10.1016/j.sedgeo.2015.11.011

Wanas, H. A., and Abdel-Maguid, N. M. (2006). Petrography and geochemistry of the CambroOrdovician Wajid Sandstone, southwest Saudi Arabia: implications for provenance and tectonic setting. *J. Asian Earth Sci.* 27, 416–429. doi:10.1016/j.jseaes.2005.05.002

Wanas, H. A., and Assal, E. M. (2021). Provenance, tectonic setting and source areapaleoweathering of sandstones of the Bahariya Formation in the Bahariya Oasis, Egypt: an implication to paleoclimate and paleogeography of the southern NeoTethys region during Early Cenomanian. *Sediment. Geol.* 413, 105822. doi:10.1016/j.sedgeo.2020.105822

Wang, A., Wang, Z., Liu, J., Xu, N., and Li, H. (2021). The Sr/Ba ratio response to salinity in clastic sediments of the Yangtze River Delta. *Chem. Geol.* 559, 119923. doi:10.1016/j.chemgeo.2020.119923

Wei, W., and Algeo, T. J. (2020). Elemental proxies for paleosalinity analysis of ancient shales and mudrocks. *Geochem. Cosmochim. Acta* 287, 341–366. doi:10.1016/j.gca.2019.06.034

Xiao, W., Zhang, B., Yang, K., Wang, Y., Wen, S., Ma, K., et al. (2023). Geochemical characteristics of the upper permian longtan Formation from northeastern sichuan basin: implications for the depositional environment and organic matter enrichment. *Acta Geol. Sin. - Engl. Ed.* 97, 1196–1213. doi:10.1111/1755-6724.15030

Xie, G., Shen, Y., Liu, S., and Hao, W. (2018). Trace and rare earth element (REE) characteristics of mudstones from Eocene pinghu formation and Oligocene huagang Formation in xihu sag, east China sea basin: implications for provenance, depositional conditions and paleoclimate. *Mar. Petrol. Geol.* 92, 20–36. doi:10.1016/j.marpetgeo.2018.02.019

Xu, C., Shan, X., Lin, H., Hao, G., Liu, P., Wang, X., et al. (2022). The formation of early Eocene organic-rich mudstone in the western Pearl River Mouth Basin, South China: insight from paleoclimate and hydrothermal activity. *Int. J. Coal Geol.* 253, 103957. doi:10.1016/j.coal.2022.103957

Yan, K., Wang, C., Mischke, S., Wang, J., Shen, L., Yu, X., et al. (2021). Major and trace-element geochemistry of Late Cretaceous clastic rocks in the Jitai Basin, southeast China. *Sci. Rep.* 11, 13846. doi:10.1038/s41598-021-93125-8

Yang, R., Li, Y., He, F., and Wu, X. (2023). Analysing of palaeoenvironment and organic matter enrichment: a case study from the Triassic Yanchang Formation in the southern Ordos Basin, China. *Geol. J.* 59 (2), 732–745. doi:10.1002/gj.4889

Zaid, S. M. (2012). Provenance, diagenesis, tectonic setting and geochemistry of rudies sandstone (lower miocene), warda field, gulf of suez, Egypt. *J. Afr. Earth Sci.* 66-67, 56–71. doi:10.1016/j.jafrearsci.2012.03.008

Zhang, X., Liu, L., Sun, Q., Xu, Y., Li, S., Wang, X., et al. (2023). Geochemistry of the Early Cretaceous saline lacustrine shales on the Lingshan Island, East China: implications for provenance, tectonic setting, and paleoweathering. *Geosci. J.* 27, 435–453. doi:10.1007/s12303-023-0010-0